J. Fluid Mech. (1990), *vol.* 215, *pp.* 161–194
Printed in Great Britain

On the connection between thin vortex layers and vortex sheets

By G. R. BAKER† AND M. J. SHELLEY‡
Program in Applied and Computational Mathematics, Princeton University, Princeton, NJ 08544, USA

(Received 17 June 1989 and in revised form 1 November 1989)

The equations for the two-dimensional motion of a layer of uniform vorticity in an incompressible, inviscid fluid are examined in the limit of small thickness. Under the right circumstances, the limit is a vortex sheet whose strength is the vorticity multiplied by the local thickness of the layer. However, vortex sheets can develop singularities in finite time, and their subsequent nature is an open question. Vortex layers, on the other hand, have motions for all time, though they may develop singularities on their boundaries. Fortunately, a material curve within the layer does exist for all time. Under certain assumptions, its limiting motion is again the vortex sheet, and thus its behaviour may indicate the nature and possible existence of the vortex sheet after the singularity time. Similar asymptotic results are obtained also for the limiting behaviour of the centre curve as defined by Moore (1978). By examining the behaviour of a sequence of layers, some physical understanding of the formation of the curvature singularity for a vortex sheet is gained. A strain flow, induced partly by the periodic extension of the sheet, causes vorticity to be advected to a certain point on the sheet rapidly enough to form the singularity. A vortex layer, however, simply bulges outwards as a consequence of incompressibility and subsequently forms a core with trailing arms that wrap around it. The evidence indicates that no singularities form on the boundary curves of the layer. Beyond the singularity time of the vortex sheet, the limiting behaviour of the vortex layers is non-uniform. Away from the vortex core, the layers converge to a smooth curve which has the appearance of a doubly branched spiral. While the circulation around the core vanishes, approximations to the vortex sheet strength become unbounded, indicating a complex, local structure whose precise nature remains undetermined.

1. Introduction

Often, the properties of vorticity are used to understand the motion of incompressible fluids (see Saffman & Baker 1979). In particular, at high Reynolds numbers the vorticity is concentrated typically in small regions and so it is tempting to use simple vorticity distributions as models for complicated flows (see Smith 1986 for applications in aerodynamics). The hope is that these vorticity distributions represent the first term of an outer expansion based on the method of matched asymptotic expansions for high-Reynolds-number flows (Van Dyke 1975). For

† Permanent address: Department of Mathematics, Ohio State University, Columbus OH 43210, USA.
‡ Permanent address: Department of Mathematics, University of Chicago, Chicago IL 60637, USA.

steady-state flows, matched asymptotic expansions have been used extensively with success, for example, in the study of boundary layers.

For unsteady flows, the construction of an asymptotic expansion for high Reynolds number is more complicated. In principle, it should be possible to construct inner and outer expansions that match at each fixed time. Conceptually, the problem is simplified if the outer expansion is a solution to Euler's equations for all time. Difficulties here are in the choice of initial conditions, in the long-time existence of the Euler solution, and in the possibility that the motion may lead to a failure of the assumptions in the asymptotic analysis.

An important special case is the narrowly confined shear layer that is shed from bodies or that occurs naturally in atmospheric or oceanic flows. A simple candidate for the outer flow for such a shear layer is a vortex sheet, whose motion is described by the Birkhoff equation. We are unaware of any work that shows that the vortex sheet is an outer flow for all time, and now recent work casts doubt upon this possibility. There is strong evidence that the sheet develops a curvature singularity in finite time. This evidence is both of a numerical and an analytical nature, and arises from studies of the two-dimensional Kelvin–Helmholtz instability. By considering a perturbation expansion in the amplitude of a small disturbance, Moore (1979) was the first to provide analytical evidence that a vortex sheet develops a curvature singularity from analytic initial data. Meiron, Baker & Orszag (1982) found results consistent with Moore's by examining the Taylor series in time constructed numerically. Using a Fourier filter to control the growth of round-off errors, Krasny (1986*a*) used the point-vortex approximation to the Birkhoff equation to study the evolution of the vortex sheet, and also found results consistent with Moore's. He found that the point-vortex approximation converged up to, but not beyond, the singularity time. On the other hand, Higdon & Pozrikidis (1985), using a different numerical method, claimed that the singularity forms as a consequence of a tightening spiral, with diverging vortex sheet strength at the spiral centre. This is in contradiction with Moore's subsequent (1985) analysis of his asymptotic equations, and the numerical results of Meiron *et al.* (1982), and Krasny (1986*a*), which indicate a finite vortex sheet strength at the singularity time.

Unfortunately, the precise form of the singularity has not yet been demonstrated analytically. There are some analytic results. Local existence of vortex sheet motion from analytic initial data has been established by Sulem *et al.* (1981). They have also shown that the motion is well-posed if restricted to analytic functions. Caflisch & Orellana (1986*a*) have established a lower bound on the time of singularity formation for sufficiently small initial data. There are specific examples of vortex sheet motion where a curvature singularity develops in finite time from analytic initial conditions (Caflisch & Orellana 1986*b*; Duchon & Robert 1989); these examples establish that the motion is ill-posed in certain non-analytic function spaces (Caflisch & Orellana 1986*b*). Note that a vortex sheet is a singular distribution of vorticity and makes sense only as a weak solution to the Euler equations. The well-developed existence and uniqueness theory for smooth solutions of the two-dimensional Euler equations is not applicable here (see, for example, McGrath 1967). There is rigorous theory establishing the existence of measure-valued solutions to the evolution of vortex sheets as described by the Euler equations (Diperna & Majda 1987). However, the concept of a measure-valued solution is so general that it provides little information about its specific nature.

Because consistent discretizations of the Birkhoff equation have failed to yield reliable results past the singularity time, alternative approaches have been adopted.

Krasny (1986*b*) modified the Biot–Savart integral, replacing the singular integrand by a smooth one. A smoothing parameter, δ, is kept fixed while the time step and number of points are varied to obtain a converged solution, which has the form of a doubly branched spiral past the singularity time. When the smoothing parameter is decreased, the outer turns of the spiral suffer little change, but there are many more turns in the inner part. These results raise the possibility that the vortex sheet is a doubly branched spiral. The uncertainty in this conjecture stems from the spatial non-uniformity in the innermost region of the spiral as δ is decreased. Thus the limit may not exist or have simple form. One might expect the spiral to be self-similar near its centre, but the only known similarity solutions for vortex sheet motion have an infinite vortex sheet strength at the moment of formation of the spiral, presumably at the singularity time (Pullin & Phillips 1981). This is contrary to the nature of the singularity in the vortex sheet for the Kelvin–Helmholtz instability. Further possibilities are that a self-similar spiral in the presence of a strain flow may have the right behaviour near its centre (D. I. Pullin, private communication), or that the spiral is not self-similar.

The approach adopted in this paper is to use smoother solutions to Euler's equations and study their limiting behaviour as a means to uncover the nature of the vortex sheet. Specifically, the vortex sheet is replaced by a layer of finite thickness and uniform vorticity. This model has several advantages. Yudovich (1963) has proven the global existence and uniqueness in time for such vorticity distributions. Moore (1978) has shown that the vortex layer approaches a vortex sheet asymptotically under the right conditions. The flow may be computed via the method of contour dynamics (Zabusky, Hughes & Roberts 1979; Pullin 1981; Pullin & Jacobs 1986). Since viscosity diffuses a shear layer, the vortex layer may be regarded as a macroscopic model for the behaviour of a thin, viscous shear layer. In §2 we present the equations of motion for the vortex layer and vortex sheet, and in the following section, we describe the asymptotic relationship between thin vortex layers and vortex sheets.

The motion of a thin vortex layer is interesting in its own right. Yudovich's theory does not exclude the interfaces bounding the vorticity from acquiring singularities, such as corners or cusps, in a finite time. A. Majda (private communication) has shown that the layer interfaces will remain smooth for small times. Pozrikidis & Higdon (1985), using the method of contour dynamics, have studied numerically the motion of periodic vortex layers, and observed the roll-up of the vorticity into roughly elliptical cores with thin trailing braids. High curvature grows rapidly where the braids attach to the core, but they did not present any quantitative analysis of the behaviour of curvature. One possibility is that curvature singularities develop on the bounding curves in finite time and that these singularities become the vortex sheet singularity in the limit of vanishing thickness. In §4 we describe the numerical techniques that we use to study the evolution of thin vortex layers, and the numerical evidence, presented in §5, suggests strongly that the singularity in the vortex sheet is not the limit of any type of singularity in the bounding interfaces of the vortex layer.

The major focus of this study is to examine the limiting behaviour of the motion of a family of vortex layers with decreasing thickness. Moore (1978) has shown that the curve lying midway between the interfaces becomes a vortex sheet in the limit of vanishing thickness, whose strength is proportional to the local thickness of the layer. His asymptotic analysis is based on the construction of an inner, local flow near the layer and an outer, far-field flow that are matched together. There is a

direct, formal approach based on the expansion of the integrals that describe the motion of the interfaces. This approach, adopted in §3, requires that the bounding curves lie a short distance on either side of some curve internal to the layer. For layers with smaller and smaller thicknesses, the bounding curves and the internal curve should approach a limiting curve. As a start, the internal curve is chosen to be the limit curve and it is assumed that it is a vortex sheet of known strength. Then the vortex layer must have a local thickness proportional to the vortex sheet strength if it is to behave asymptotically like the vortex sheet. This result provides the framework for the numerical study conducted in §§5 and 6; a family of vortex layers are chosen so that their initial thicknesses are proportional to the strength of a given vortex sheet and the motion of the layers is computed numerically.

The results show a major difference between the motion of a thin vortex layer and its approximation by the motion of a vortex sheet. Briefly, in both cases a straining flow drives the vorticity towards an accumulation point that becomes the point of curvature singularity for the vortex sheet. The layer, on the other hand, bulges owing to incompressibility. The bulge in the layer reorganizes into a rotating, roughly elliptical core about which trailing arms wrap. For thinner layers, the core is smaller and forms closer to the singularity time, while the trailing arms wrap further around the core. It is difficult to extrapolate the limiting form for the layer from this behaviour.

Given the uncertainty in the relationship between the vortex sheet and the limiting curve beyond the singularity time, it is valuable to choose different internal curves whose existence is independent of that of the vortex sheet. Moore (1978) used the centre curve, and we use his results as a check on the validity of our asymptotic expansions. Another choice is the material curve whose global existence is assured by the theory of Yudovich (1963). In both cases, the internal curves become vortex sheets asymptotically. These results, derived in §3, provide us with further tools, used in §6, to study the properties of the limiting curve. Before the singularity time, the centre curve and the material curve both converge to the vortex sheet. After the singularity time, the convergence is non-uniform, and so reliable extrapolation is difficult, but the apparent limit is composed of a vortex sheet in the form of a doubly branched spiral where the trailing arms occur and a point of infinite vortex sheet strength, but no net circulation, where the cores occur.

Finally, we discuss the relevance of our results and present our conclusions in §7.

2. The equations of motion

In terms of the vorticity, ω, and the stream function, ψ, the two-dimensional motion of an inviscid, incompressible fluid of constant density is governed by

$$\frac{\mathrm{D}\omega}{\mathrm{D}t} = 0, \tag{2.1a}$$

$$\Delta\psi = -\omega, \tag{2.1b}$$

$$u = \frac{\partial\psi}{\partial y}, \quad v = -\frac{\partial\psi}{\partial x}, \tag{2.1c}$$

where u and v are the components of the velocity field. A simple weak solution to these equations consists of a region of constant vorticity embedded in irrotational flow, with the velocity continuous across the interfaces bounding the region. Zabusky

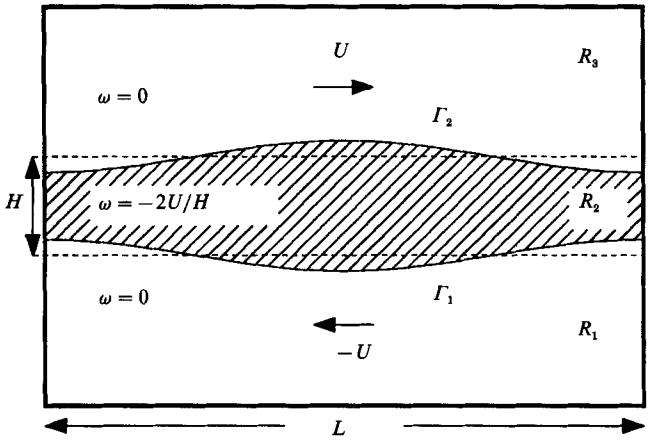

FIGURE 1. A schematic of the vortex layer.

et al. (1979) noted that for such flows the motion is determined completely by the location of the interfaces.

For a periodic layer of constant vorticity, Pozrikidis & Higdon (1985) followed Zabusky *et al.* (1979) in expressing the velocity of the fluid in terms of a source distribution along each interface. We follow Pullin (1981), Broadbent & Moore (1985) and Pullin & Jacobs (1986) in expressing the velocity in terms of a dipole distribution along each interface. This formulation is the most convenient for an asymptotic analysis of thin layers and has certain computational advantages as well.

The vorticity region considered here is a periodic layer as shown in figure 1, with mean width H, periodic length L (we take $L = 2\pi$ without loss of generality), and vorticity $-2U/H$ (this implies $(u, v) \to (\pm U, 0)$ as $y \to \pm\infty$). Let the lower interface, Γ_1, be parametrized as $z_1(p)$, and the upper interface, Γ_2, as $z_2(p)$, where $z_j(p) = x_j(p) + \mathrm{i}y_j(p)$, $-\infty \leqslant p \leqslant +\infty$, and $z_j(p+2\pi) = 2\pi + z_j(p)$. R_1, R_2, and R_3 denote the lower, middle, and upper regions, respectively. The complex fluid velocity, $w = u + \mathrm{i}v$, at a field point $\eta = x + \mathrm{i}y$ is given in the compact form,

$$w^*(\eta, t) = \frac{2U}{H}\int_0^{2\pi} (y_1(q,t) - y)\,\mathrm{P}(\eta, z_1(q,t))\, z_{1q}(q,t)\,\mathrm{d}q$$
$$-\frac{2U}{H}\int_0^{2\pi} (y_2(q,t) - y)\,\mathrm{P}(\eta, z_2(q,t))\, z_{2q}(q,t)\,\mathrm{d}q. \quad (2.2)$$

The asterisk superscript refers to complex conjugation, the q subscript refers to differentiation, and

$$\mathrm{P}(\eta, z) = \frac{1}{4\pi\mathrm{i}}\cot\frac{\eta - z}{2}. \quad (2.3)$$

A derivation of (2.2) is given in Pullin & Jacobs (1986). Since the interfaces must move with the fluid velocity, their equations of motion follow by setting $\eta = z_j(p, t)$, or

$$\frac{\partial z_1}{\partial t}(p,t) = w_1(p,t) \equiv w(z_1(p,t)), \quad (2.4a)$$

$$\frac{\partial z_2}{\partial t}(p,t) = w_2(p,t) \equiv w(z_2(p,t)), \quad (2.4b)$$

where the partial time derivatives are taken keeping the Lagrangian variable, p, fixed. The set of evolution equations for the interfaces, (2.2) and (2.4), requires knowledge of the location of the interfaces only.

The Lagrangian motion, as defined by (2.4), is inconvenient for both computational and asymptotic purposes, since points on the interfaces advect indefinitely to the right or left as a consequence of the shear. It is preferable to keep the computational points trapped inside a periodic window, and so a tangential speed V_j is added to fix the first point at $x(p=0)=0$. Thus, (2.4) is replaced by

$$\frac{\partial z_j}{\partial t}(p,t) = w_j(p,t) - V_j \frac{z_{jp}(p,t)}{s_{jp}(p,t)}, \tag{2.5}$$

where V_j is determined by the condition $u_j(0,t) = V_j x_{jp}(0,t)/s_{jp}(0,t)$, and $s_{jp}(p,t) = |z_{jp}(p,t)|$.

A simple steady state for the motion of the vortex layer is given by $y_1 = -\frac{1}{2}H$ and $y_2 = \frac{1}{2}H$. This steady state is linearly unstable to perturbations of the form

$$x_1 = p + \frac{U}{H\sigma} e^{\sigma t}\{A_1[e^{-2kH} - 1 + kH] + A_2 kH\, e^{-kH}\}(\cos kp - 1) + e^{\sigma t}\{A_1 - A_2 e^{-kH}\}\sin kp, \tag{2.6a}$$

$$x_2 = p - \frac{U}{H\sigma} e^{\sigma t}\{A_1 kH\, e^{-kH} + A_2[e^{-2kH} - 1 + kH]\}(\cos kp - 1) + e^{\sigma t}\{-A_1 e^{-kH} + A_2\}\sin kp, \tag{2.6b}$$

$$y_1 = -\tfrac{1}{2}H + e^{\sigma t}\{-A_1[1 - kH] + A_2 e^{-kH}\}\cos kp + e^{\sigma t}\frac{H\sigma}{U} A_1 \sin kp, \tag{2.6c}$$

$$y_2 = \tfrac{1}{2}H + e^{\sigma t}\{-A_1 e^{-kH} + A_2[1 - kH]\}\cos kp + e^{\sigma t}\frac{H\sigma}{U} A_2 \sin kp, \tag{2.6d}$$

where the growth rate σ is given by

$$\sigma^2 = \frac{U^2}{H^2}[e^{-2kH} - (1 - kH)^2]. \tag{2.7}$$

The maximum growth rate $\sigma_m \approx 0.4U/H$ occurs when $kH \approx 0.8$. When $kH > 1 + \exp(-kH)$, the perturbation is neutrally stable. These results were first obtained by Rayleigh (1880), who was very concerned about the ill-posedness of vortex sheet motion and its regularization by a thin layer of finite thickness.

The motion of a vortex sheet, parametrized by a Lagrangian variable p as $z(p,t)$, is given by the Birkhoff–Rott equation

$$\frac{\partial z^*}{\partial t}(p,t) = P\int_0^{2\pi} \gamma(q,t)\, \mathrm{P}(z(p,t), z(q,t))\, s_q(q,t)\, \mathrm{d}q, \tag{2.8a}$$

where the integral is a principal-value one, and γ is the vortex sheet strength, satisfying

$$\frac{\partial}{\partial t}(\gamma(p,t)\, s_p(p,t)) = 0. \tag{2.8b}$$

This equation expresses the conservation of circulation along the sheet.

A steady state for the motion of the vortex sheet is given by $y = 0$ and $\gamma = -2U$, but it is always linearly unstable to perturbations of the form

$$x = p + \frac{b}{k}\cos kp - \frac{a}{k}\sin kp + \frac{Uk}{\sigma}e^{\sigma t}\{A_1 \cos kp + A_2 \sin kp\}, \tag{2.9a}$$

$$y = e^{\sigma t}\{A_1 \cos kp + A_2 \sin kp\}, \tag{2.9b}$$

$$\gamma s_p = -2U(1 - a\cos kp - b\sin kp), \tag{2.9c}$$

which the growth rate σ is given by

$$\sigma^2 = U^2k^2. \tag{2.10}$$

Note that the limit of (2.7) as $H \to 0$ is (2.10), indicating how a thin vortex layer might be an appropriate regularization of a vortex sheet, but these results do not reveal clearly the general connection between vortex layers of vanishing thickness and vortex sheets. This is the subject of the next section.

3. Asymptotic expansions for small thickness

In this section, the evolution of thin vortex layers will be studied in the limit of vanishing mean thickness. At any fixed time, the two bounding curves of a vortex layer should converge to a limiting curve. Since the general properties of the bounding curves, such as the continuity of their normals, are not known as they evolve, little can be said about the nature of the limiting curve. Even if the bounding curves are assumed to be analytic for all time, it is not necessary that the limiting curve will be analytic. Thus it will be necessary to make some assumptions in order to derive a perturbation expansion.

As a starting point for the analysis of the behaviour of thin layers, the bounding curves may be considered to lie a short distance on either side of the limiting curve. However, the Lagrangian motion of points on the bounding curves may result in their displacement tangentially to the limiting curve. Consequently, the use of a parametrization based on Lagrangian motion is inconvenient. Instead, a new parametrization is introduced to ensure that points on either bounding curve with the same label will converge to the same point on the limiting curve. The idea is to express the bounding curves in terms of their distance along the normal to the limiting curve. The definition for the motion of points on the bounding curves must be modified so that a point on either bounding curve normal to a particular point on the limiting curve will remain so subsequently.

A further generalization is needed. One expects the limiting curve to be a vortex sheet up to the time of singularity formation, but beyond that time the nature and even the existence of the vortex sheet is in question. A major motivation for this study is to determine the nature of the limiting curve beyond the time of singularity formation, for if the limiting curve is well-defined and smooth, then presumably it is a vortex sheet. On the other hand, if the limiting curve does not have a continuous normal, then its use as an agent to establish the parametrization of the bounding curves is invalid. Therefore it is useful to consider the limiting behaviour of certain curves defined within the vortex layer, for example the centre curve as defined by Moore (1978) or a material curve that moves with the fluid. Either of these internal curves may be used in place of the limiting curve as the way to define the parametrization of the bounding curves. The study of the limiting form for the layer and the internal curve can then be done simultaneously. The advantage of this

approach is that no guess is required for the limiting curve. Also, a material curve has a well-defined motion for all time, and so one may hope that a limiting material curve may exist for all time.

Let $\bar{z}$ lie within the vortex layer and be either a vortex sheet, a centre curve, or a material curve. The bounding curves are assumed to have the form

$$z_1(p) = \bar{z}(p) - \mathrm{i}H_1(p)\frac{\bar{z}_p(p)}{\bar{s}_p(p)}, \tag{3.1a}$$

$$z_2(p) = \bar{z}(p) + \mathrm{i}H_2(p)\frac{\bar{z}_p(p)}{\bar{s}_p(p)}. \tag{3.1b}$$

For convenience, explicit time dependence will not be shown. The real-valued functions H_1 and H_2 give the distance of the bounding curves to $\bar{z}$ along its normal and are assumed to be single-valued and smooth. A schematic is given in figure 2.

The motion of a point, labelled p, on one of the bounding curves, labelled j, will no longer be with the fluid flow. Let $w_j(p)$ be the fluid velocity at that point; namely, $w_j(p) = w(z_j(p))$. Then the motion of the point will be given by

$$\frac{\partial z_j}{\partial t}(p) = w_j(p) + \alpha_j(p)\frac{z_{jp}(p)}{s_{jp}(p)}, \tag{3.2}$$

where α_j is a real parameter controlling the speed that must be added to the fluid velocity along the tangent to the bounding curve so that the point remains on the normal to the internal curve at $\bar{z}(p)$. The motion in the normal direction of any point on the bounding curves will be that of the fluid, for kinematic reasons.

For layers with small mean thickness, H, the following expansions are assumed:

$$H_j(p) = h_{j1}(p)H + h_{j2}(p)H^2 + O(H^3), \tag{3.3a}$$

$$\alpha_j(p) = \alpha_{j0}(p) + \alpha_{j1}(p)H + O(H^2), \tag{3.3b}$$

$$w_j(p) = w_{j0}(p) + w_{j1}(p)H + O(H^2), \tag{3.3c}$$

$$\bar{z}(p) = z(p) + \hat{z}_1(p)H + \hat{z}_2(p)H^2 + O(H^3), \tag{3.3d}$$

$$\bar{w}(p) = w(p) + \hat{w}_1(p)H + O(H^2). \tag{3.3e}$$

We define also $T_k = h_{1k} + h_{2k}$, and $\Delta h_k = h_{1k} - h_{2k}$. Note that the internal curve, $\bar{z}$, trapped between the bounding curves, must also converge to the limiting curve, z, but an additional assumption is made; the parametrization of $\bar{z}$ must be well-defined in the limit of vanishing thickness. There are simple examples where this is not the case. Consider $\bar{z}(p) = p + 2\sin(p) + \mathrm{i}H\sin(p)$. This curve is well-defined for $H > 0$, but when $H = 0$, the limiting curve is obviously $y = 0$, although the parametrization fails since $s_p(p) = |x_p(p)|$ has zeros.

The above expansions are substituted into (3.1) and (3.2) and terms up to $O(H^2)$ are retained. The integrands in (2.2) must be expanded to $O(H^3)$ in order to obtain the expansion for the complex velocity to $O(H^2)$. Details have been omitted, but are available from the authors in the form of a report. We present here only the results.

We start by assuming that the limiting curve is a vortex sheet and by choosing the internal curve to be that vortex sheet. In this case, $\bar{w}$ and $\bar{z}$ are independent of H, so $\hat{w}_j = 0$ and $\hat{z}_j = 0$ for $j > 0$. Furthermore,

$$w^*(p) = P\int_0^{2\pi} \gamma(q)\,\mathrm{P}(z(p), z(q))\,s_q(q)\,\mathrm{d}q, \tag{3.4}$$

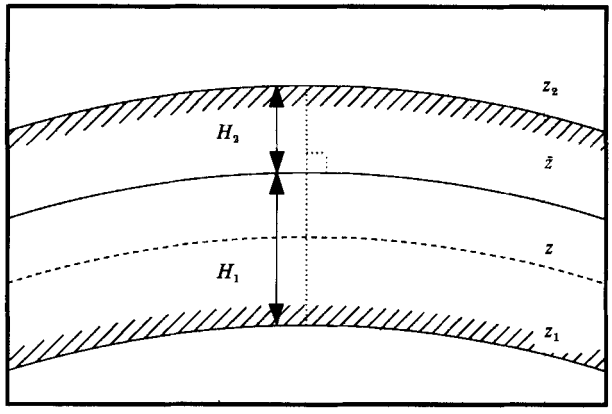

FIGURE 2. An illustration of the notation.

where γ is the vortex sheet strength. To lowest order, the motion of the layer becomes that of the vortex sheet provided

$$2UT_1 = -\gamma, \quad \alpha_{j0} = \pm UT_1. \tag{3.5a, b}$$

The upper and lower signs correspond to $j = 1$ and 2 respectively. The result in (3.5a) makes physical sense. It states that the vortex sheet strength is the product of the vorticity ($-2U/H$) and the local thickness (to leading order $T_1 H$). The results at the next order give an evolution equation for T_1:

$$\frac{\partial T_1}{\partial t} s_p + T_1 s_p \operatorname{Re}\left\{\frac{w_p}{z_p}\right\} = \frac{\partial}{\partial t}(T_1 s_p) = 0. \tag{3.6}$$

Since T_1 is proportional to γ, (3.6) gives the correct statement of the conservation of circulation along a vortex sheet.

Clearly then, if the vortex sheet exists, the motion of the finite layer will converge to it in the limit of vanishing thickness. However, it is the existence and nature of the sheet that is at question and so this result is most useful in specifying the initial conditions when the vortex sheet is replaced by vortex layers. Their local thicknesses must scale appropriately with the vortex sheet strength. The early motion should still converge to the vortex sheet, but when the sheet reaches a curvature singularity, it is no longer clear that the asymptotic procedure remains valid. Instead, the motion of other curves, also lying inside the layer, may be studied in the limit of vanishing thickness.

We consider next the centre curve as defined by Moore (1978). The centre curve has the property that the bounding curves lie an equal distance on either side of it along its normal; thus $H_1 = H_2$, or $\Delta h_j = 0$. However, its complex velocity w^* must be determined. The results at lowest order are

$$\alpha_{j0} = C \pm UT_1, \tag{3.7a}$$

where the upper, lower sign correspond to $j = 1, 2$ respectively. Also

$$w^*(p) = -P\int_0^{2\pi} 2UT_1(q)\,\mathrm{P}(z(p), z(q))\, s_q(q)\,\mathrm{d}q + C\frac{z_p^*(p)}{s_p(p)}, \tag{3.7b}$$

which is the motion of a vortex sheet of strength $-2UT_1$, with an arbitrary tangential speed, C, which may depend on p and t. The presence of C arises from the fact that

the lowest-order equations form a singular system. One would normally expect a compatibility condition applied to the system of equations at next order, to determine C. However, the compatibility condition is automatically satisfied and one finds

$$\frac{\partial T_1}{\partial t} s_p + T_1 s_p \operatorname{Re}\left\{\frac{w_p}{z_p}\right\} - \frac{\partial}{\partial p}(CT_1) = 0, \tag{3.8}$$

which is the correct statement of conservation under the motion of the curve given by (3.7b). That the variable C is not determined reflects the lack of definition for the parametrization of the centre curve. Any curve may have its parametrization changed by a variable shift along its tangent. Moore (1978) fixes the parametrization of the boundary curves and so the parametrization of his centre curve is determined. We are free to specify C and the easiest choice is to set it to zero. The general solution for the first-order correction to the complex velocity of the centre curve is

$$\hat{w}_1^*(p) = U\left(i\frac{T_1(p)\,T_{1p}(p)}{s_p(p)} + \frac{T_1^2(p)\,\kappa(p)}{2}\right)\frac{z_p^*(p)}{s_p(p)} + A\frac{z_p^*(p)}{s_p(p)} + P\int_0^{2\pi} U\tau(p,q)\,\mathrm{P}(z(p),z(q))\,\mathrm{d}q, \tag{3.9}$$

where

$$\tau(p,q) = -T_2(q)\,s_q(q) + \mathrm{i}T_1(q)\,s_q(q)\,\mathrm{Im}\left\{\frac{\hat{z}_{1q}(q)}{z_q(q)}\right\},$$

and κ is the curvature:

$$\kappa = \mathrm{Im}\left\{\frac{z_{pp}\,z_p^*}{s_p^3}\right\}.$$

Again, the motion is arbitrary to some tangential speed, A. Presumably, the application of the compatibility condition to the next-order equations would determine A, but we find the calculation too formidable. Instead, our results are compared to Moore's (1978). He wrote his results, correct to $O(H^2)$, as the motion of a vortex sheet plus a correction term. In our variables, Moore's result is

$$\frac{\partial \bar{z}^*}{\partial t}(p) = P\int_0^{2\pi} \bar{\gamma}(q)\,\mathrm{P}(\bar{z}(p),\bar{z}(q))\,\bar{s}_q(q)\,\mathrm{d}q + \frac{H\bar{\gamma}(p)}{4U}\left(\mathrm{i}\frac{\bar{\gamma}_p(p)}{\bar{s}_p(p)} + \tfrac{1}{2}\bar{\gamma}(p)\,\bar{\kappa}(p)\right)\frac{\bar{z}_p(p)}{\bar{s}_p(p)}, \tag{3.10}$$

where $\bar{\gamma} = -2U(T_1 + HT_2)$, and $\bar{\kappa} = \mathrm{Im}\{\bar{z}_{pp}\,\bar{z}_p^*/\bar{s}_p^3\}$. Our results are

$$\frac{\partial \bar{z}^*}{\partial t}(p) = P\int_0^{2\pi} \bar{\gamma}(q)\,\mathrm{P}(\bar{z}(p),\bar{z}(q))\,\bar{s}_q(q)\,\mathrm{d}q + \frac{H\bar{\gamma}(p)}{4U}\left(\mathrm{i}\frac{\bar{\gamma}_p(p)}{\bar{s}_p(p)} + \tfrac{1}{2}\bar{\gamma}(p)\,\bar{\kappa}(p) + 4U\frac{A(p)}{\bar{\gamma}(p)}\right)\frac{\bar{z}_p(p)}{\bar{s}_p(p)}, \tag{3.11}$$

and there is complete agreement with Moore's result if $A = -\bar{\kappa}\bar{\gamma}^2/24U$. Since A has not been determined, all that can be stated is that there are no inconsistencies between the results.

Finally we turn to the third choice for the motion of the curve internal to the layer, a material curve. A material curve is composed of points that follow the motion of the fluid; hence,

$$\frac{\partial \bar{z}}{\partial t}(p) = \bar{w}(p) \equiv w(\bar{z}(p)), \tag{3.12}$$

where $w(\bar{z})$ is given by (2.2). The results at lowest order are

$$\alpha_{j0} = U(\Delta h_1 \pm T_1), \tag{3.13a}$$

where the upper, lower signs correspond to $j = 1, 2$ respectively. Also,

$$w^*(p) = U\Delta h_1 \frac{z_p^*(p)}{s_p(p)} - P\int_0^{2\pi} UT_1(q)\,\mathrm{P}(z(p), z(q))\, s_q(q)\,\mathrm{d}q, \tag{3.13b}$$

which is the motion of a vortex sheet of strength $-2UT_1$. The equations at the next order give the result

$$\frac{\partial T_1}{\partial t} s_p + T_1 s_p \,\mathrm{Re}\left\{\frac{w_p}{z_p}\right\} - U\frac{\partial}{\partial p}(T_1 \Delta h_1) = 0, \tag{3.14}$$

which is the correct conservation equation for the circulation along the curve under the motion given by (3.13*b*).

In summary, we find that the layer and any of the chosen internal curves become a vortex sheet in the limit of vanishing mean thickness. Several assumptions are made: all curves are smooth (have at least a continuous curvature), the distances of the boundary curves from the internal curve or the limiting curve are single-valued, smooth functions of the parametrization, and all the expansions are power series in the mean thickness. In §§5 and 6, a numerical study of the evolution of the layers is conducted, and the results show that these assumptions can fail.

4. Numerical results

This section describes the numerical methods used in evolving the boundaries of the vortex layers, material curves within a layer, and vortex sheets. As shown in §2, the velocities for all of these can be expressed as boundary integrals with Cauchy kernels. The evolution equations for the layer interfaces, (2.5), are solved by the method of lines. The interfaces are represented by a distribution of points, and the differential and integral operators on the right-hand side of (2.5) are replaced by approximating discrete operators. The resulting system is then a finite set of ordinary differential equations in time, which is integrated by a fourth-order, Adams–Moulton predictor-corrector method. The Adams–Moulton method is used also to integrate the motion of vortex sheets and passive interfaces described later.

There are two main considerations in selecting a numerical method for the evaluation of the boundary integrals. One is efficiency: the number of operations required to evaluate the integrals should be as low as possible for a given level of accuracy. The other consideration is accuracy, which is particularly important in this study, since attention will focus on whether singularities form along the boundaries. Truncation errors may affect the real motion in several ways, but our primary concern is that they may diffuse or disperse the formation of singularities. If a low-order method is used, then the truncation errors do not change substantially over a few doublings in the choice of the number of quadrature points, and so its insiduous effects, if present, may be hard to detect. Consequently, we have selected a method that is highly accurate and efficient.

The boundary integrals are of two distinct types. The first integral has the form

$$I_j^{(1)}(p) = \int_0^{2\pi} (y_j(q) - y_j(p))\,\mathrm{P}(z_j(p), z_j(q))\, z_{jq}(q)\,\mathrm{d}q. \tag{4.1}$$

For example, this form arises by setting η to $z_1(p)$ in the first integral in (2.2). Despite appearances, the integrand in (4.1) is a smooth, periodic function of q, because the kernel $\mathrm{P}(z(p), z(q))$ has a Cauchy-type singularity at $q = p$ which is cancelled by a compensating zero in $\mu(q) - \mu(p)$. By taking the collocation points to be uniformly

distributed in q, the integral can be evaluated with spectral or infinite-order accuracy by the trapezoidal rule over the collocation points. Accuracy is then limited by the approximation to $z_q(q)$ at the collocation points. In this work, derivatives are approximated by periodic, quintic splines with an accuracy of $O(\Delta q^6)$.

The second type of integral in (2.2) has the form

$$I_{jk}^{(2)}(p) = \int_0^{2\pi} (y_j(q) - y_k(p))\, \mathrm{P}(z_k(p), z_j(q))\, z_{jq}(q)\, \mathrm{d}q, \tag{4.2}$$

where $j \neq k$. This form arises, for example, when the field point η is set to $z_2(p)$ in the first integral in (2.2). This type of boundary integral is much more difficult to evaluate accurately. While the trapezoidal rule may still be applied over the collocation points to yield spectral accuracy formally, large errors are incurred nonetheless when the interfaces are close. Accuracy can be restored by adaptive techniques which construct new sets of quadrature points, while still preserving spectral accuracy. For details see Baker & Shelley (1986). The application of these adaptive methods requires interpolated values for $z_j(q)$ and $z_{jq}(q)$ between the collocation points. Such interpolations are accomplished by the construction of local, quintic Hermite polynomials on each subinterval of the mesh, where the necessary approximations to the derivatives at the collocation points are found by iterated, periodic, quintic splines (Shelley & Baker 1988). The overall accuracy is $O(\Delta q^6)$.

The accuracy of the calculations is checked by several different measures. First, for short times, the computed solution agrees with the approximate solution provided by a fourth-order perturbation expansion to within the accuracy of the expansion. At intermediate times, convergence of the calculation is verified by monitoring the point-wise convergence of the layer interfaces as both the spatial and temporal resolution are varied systematically. The area and first moments of a periodic segment, and the perturbation kinetic energy, are constants of the motion that are monitored. We find that the error in the perturbation kinetic energy, whose calculation is described in Appendix A, consistently overestimates the point-wise error of the numerical solution. If this relationship is generally correct, then our calculations are correct to within five digits even at long times, when costs make studies of point-wise convergence too expensive. The other constants of the motion are conserved well by our calculations, but of course these global error estimates cannot guarantee point-wise accuracy. The errors in these constants are given later with the details of specific calculations.

As will be seen in the next section, the motion of the vortex layer leads to the formation of regions of high curvature, and regions of stretching in the bounding interfaces. To maintain resolution of the interfaces, and consequently accuracy, the mesh is redistributed periodically to resolve the regions of high curvature, and to keep collocation points in the regions of rapid stretching. The mesh redistribution is based on the concept of an 'equidistribution' of a function which measures (in some sense) the variation of the solution. Details of the equidistribution method and its implementation are given in Appendix B. It should be noted that the mesh redistribution is not of the insert-and-delete type, which leads to non-smooth meshes, but instead finds a smooth reparameterization for the interfaces.

In §6, the limiting behaviour of the vortex layer will be studied. For this, the motion of material curves and of vortex sheets must be computed. The velocity at a point $z(p,t)$ on a material curve is given by

$$\frac{\partial z}{\partial t}(p,t) = w(z(p,t)), \tag{4.3}$$

where w is the fluid velocity, as given by (2.2). The evaluation of integrals of a similar form to (4.2) is required, and is done by the adaptive quadrature methods discussed above.

The evolution of a periodic vortex sheet is governed by the periodic form of the Birkhoff–Rott equation given in (2.8). Shelley (1990) shows that the trapezoidal rule using alternate points gives a spectrally accurate approximation to the Birkhoff–Rott integral. Because of sensitivity to round-off errors (Krasny 1986*a*), calculations are done with a precision of 29 digits and a spectral filter is used to prevent the rapid growth of the smallest-scale modes introduced by round-off errors. The computed solution is checked at early times against the solution obtained from the Taylor series in time derived by Meiron *et al.* (1982). The results obtained this way (Shelley 1990) are an improvement on the results obtained by Krasny and Meiron *et al.*, especially at times shortly before the singularity time.

5. The evolution and regularity of the vortex layer

The initial conditions considered here are of the form

$$z_1(p, t=0) = p - \mathrm{i}\tfrac{1}{2}H(1 - a\cos p), \tag{5.1a}$$

$$z_2(p, t=0) = p + \mathrm{i}\tfrac{1}{2}H(1 - a\cos p), \tag{5.1b}$$

with $a < 1$. The motivation for this choice lies in the results given in §3; the limit of (5.1) and (2.4) as $H \to 0$, while U (or equivalently the circulation around a periodic segment) is held fixed, is a vortex sheet at

$$z(p) = p, \tag{5.2a}$$

with strength

$$\gamma(p) = -2U(1 - a\cos p). \tag{5.2b}$$

For $a \ll 1$, the linear motion of the vortex layer with initial condition (5.1) may be determined from (2.6) as

$$x_1 = p + \frac{Ua}{2\sigma}\sinh\sigma t(\cos p - 1) + \frac{Ha}{2D}(1 - \mathrm{e}^{-H})(\cosh\sigma t - 1)\sin p, \tag{5.3a}$$

$$x_2 = p - \frac{Ua}{2\sigma}\sinh\sigma t(\cos p - 1) + \frac{Ha}{2D}(1 - \mathrm{e}^{-H})(\cosh\sigma t - 1)\sin p, \tag{5.3b}$$

$$y_1 = -\tfrac{1}{2}H + \tfrac{1}{2}Ha\cosh\sigma t\cos p + \frac{a\sigma H^2}{2UD}\sinh\sigma t\sin p, \tag{5.3c}$$

$$y_2 = \tfrac{1}{2}H - \tfrac{1}{2}Ha\cosh\sigma t\cos p + \frac{a\sigma H^2}{2UD}\sinh\sigma t\sin p, \tag{5.3d}$$

where σ is the real, positive root of $H^2\sigma^2 = U^2[\mathrm{e}^{-2H} - (1-H)^2]$ (this requires $H < 1.2$), and $D = \mathrm{e}^{-H} - 1 + H$. The centre curve for the linear motion of the layer may be determined approximately within the assumptions of linear theory (see Appendix C), and, as $H \to 0$, it agrees with the linear motion of the vortex sheet with initial condition (5.2):

$$z = p - a(1 - \cosh Ut - \mathrm{i}\sinh Ut)\sin p. \tag{5.4}$$

Besides illustrating some aspects of the asymptotic results in §3, the linear results show how the unstable motion of the layer relates to that of the vortex sheet. In particular, perturbations of the layer that have equal amplitudes in the disturbance

H	N	Δt	T	ΔT	k_i
0.20	512	0.01	4.70	0.1	4, 6, 7, 9
0.10	512	0.005	3.45	0.05	5, 6, 7, ...
0.05	512	0.0025	2.60	0.05	3, 5, 6, 7, ...
0.025	512	0.00125	2.05	0.025	7, 9, 10, 11, ...

TABLE 1. The values of the numerical parameters for the layer calculations. H is the mean thickness; N is the number of collocation points for each interface; Δt is the time step. Grid redistributions are done at times, $T + k_i \Delta T$, where T is the first time, ΔT is the smallest interval between redistributions, and k_i are positive integers. The time step is halved when $t > T$.

H	Kinetic energy	Area	x-moment	y-moment
0.20	4.42×10^{-6}	2.69×10^{-10}	4.27×10^{-13}	1.04×10^{-10}
0.10	1.89×10^{-6}	1.50×10^{-9}	2.77×10^{-11}	6.62×10^{-12}
0.05	3.98×10^{-5}	2.45×10^{-8}	1.13×10^{-11}	1.18×10^{-12}
0.025	7.66×10^{-6}	1.84×10^{-8}	4.70×10^{-11}	1.36×10^{-11}

TABLE 2. Maximum errors in the perturbation kinetic energy, and in the area and first moments of a periodic segment, incurred during each calculation listed in table 1. All errors are relative, except those for the y-moment. The y-moment is zero for these calculations.

of each interface, but are out of phase, correspond to perturbations in the strength of a flat vortex sheet. On the other hand, perturbations that are in phase correspond to perturbations in the position of vortex sheet of constant strength. General perturbations are a linear combination of these two cases.

Meiron *et al.* (1982, subsequently referred to as MBO) examined the singularity structure of a vortex sheet evolving from the initial condition (5.2), and found strong evidence to indicate that such a vortex sheet loses its analyticity at a finite time. In a periodic interval, $0 \leqslant p \leqslant 2\pi$, the vortex sheet acquires a curvature singularity at $p = \pi$. MBO found an asymptotic estimate for the critical time, t_c, based on the analysis of Moore (1979), but the numerical results of both MBO and Shelley (1990) suggest that the asymptotic result is an underestimate. We select $U = \frac{1}{2}$, $a = \frac{1}{2}$ as values that lead to the formation of the singularity in a reasonable time. In fact, the highly accurate results of Shelley (1990) give $t_c = 1.615 \pm 0.010$, whereas Moore's asymptotic estimate is $t_c \approx 1.44$. The estimate found by MBO is $t_c \approx 1.6$. The evolution of vortex layers with $U = \frac{1}{2}$ and $a = \frac{1}{2}$ is calculated numerically for various mean thicknesses, $H = 0.025$, 0.05, 0.1, and 0.2. Table 1 lists the choice of the numerical parameters for each calculation with finest resolution. Note that the number of collocation points is large enough that all growing modes, according to linear theory, are represented in the calculations. Table 2 lists the maximum errors incurred during each calculation in the perturbation kinetic energy, and in the area and first moments of a periodic segment of the layer. Clearly our calculations have a high degree of accuracy. The case $H = 0.025$ corresponds to an aspect ratio of 250 to 1, and is the thinnest layer our numerical method can compute reliably. The reason why it is difficult to calculate the motion of thinner layers may be understood heuristically from linear theory. The most unstable disturbance grows at a rate $0.4U/H$, and it will affect the motion of the layer before t_c if its initial amplitude exceeds $a_0 = H \exp(-0.64/H)$. For $H = 0.025$, $a_0 \approx 2 \times 10^{-13}$ and is close to the order

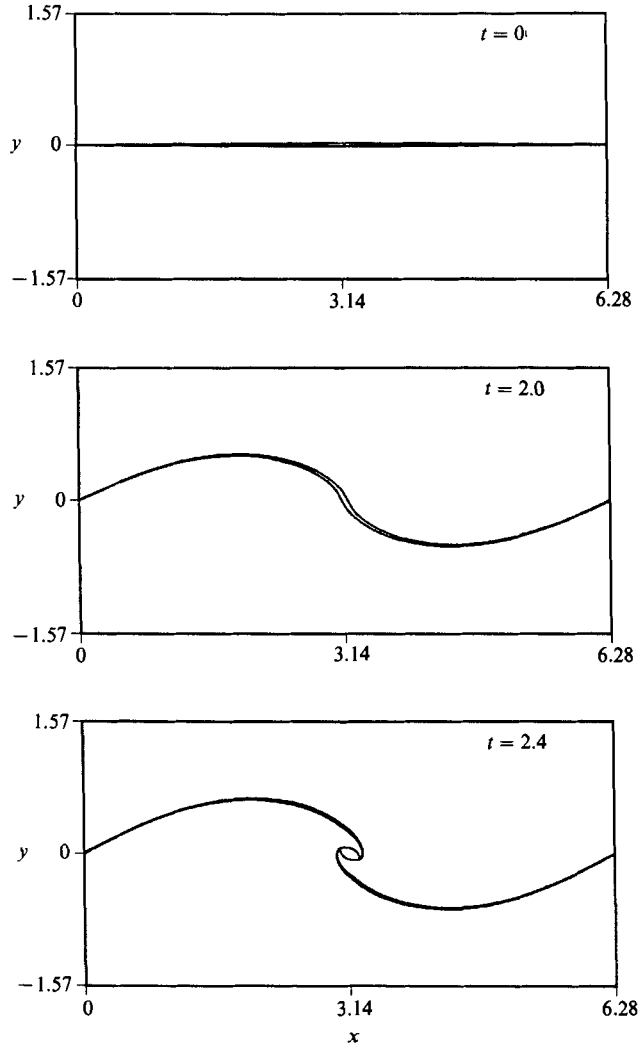

FIGURE 3. The location of the layer interfaces for $H = 0.025$ at various times.

of the round-off error committed on a Cray computer. Our attempts to calculate a layer with $H = 0.0125$ failed owing to the appearance of round-off errors.

Figure 3 shows the location of the layer interfaces with $H = 0.025$ at various times, $t = 0$, 2.0 and 2.4. The location of the interfaces for a thicker layer, $H = 0.1$, is shown in figure 4 at times, $t = 0$, 2.0, 2.4, and 4.0. The evolution occurs in three phases. First, the vorticity advects to the centre (at $p = \pi$), causing a further thickening there due to incompressibility. Second, the vorticity in the centre quickly reforms into a roughly elliptical core with trailing arms, which subsequently wrap around the core as it revolves. It is possible that these cores are similar to the rotating ellipses found by Kida (1981) that exist in an external strain flow, the strain flow in this case being induced in part by the periodic extensions of the layer. The aspect ratio of the cores falls within the 3:1 linear stability requirement given by Love (1883) for Kirchhoff ellipses, but the more relevant stability condition might be that of rotating ellipses in a strain flow (see Dritschel 1990). We note also that the smaller the value of H, the

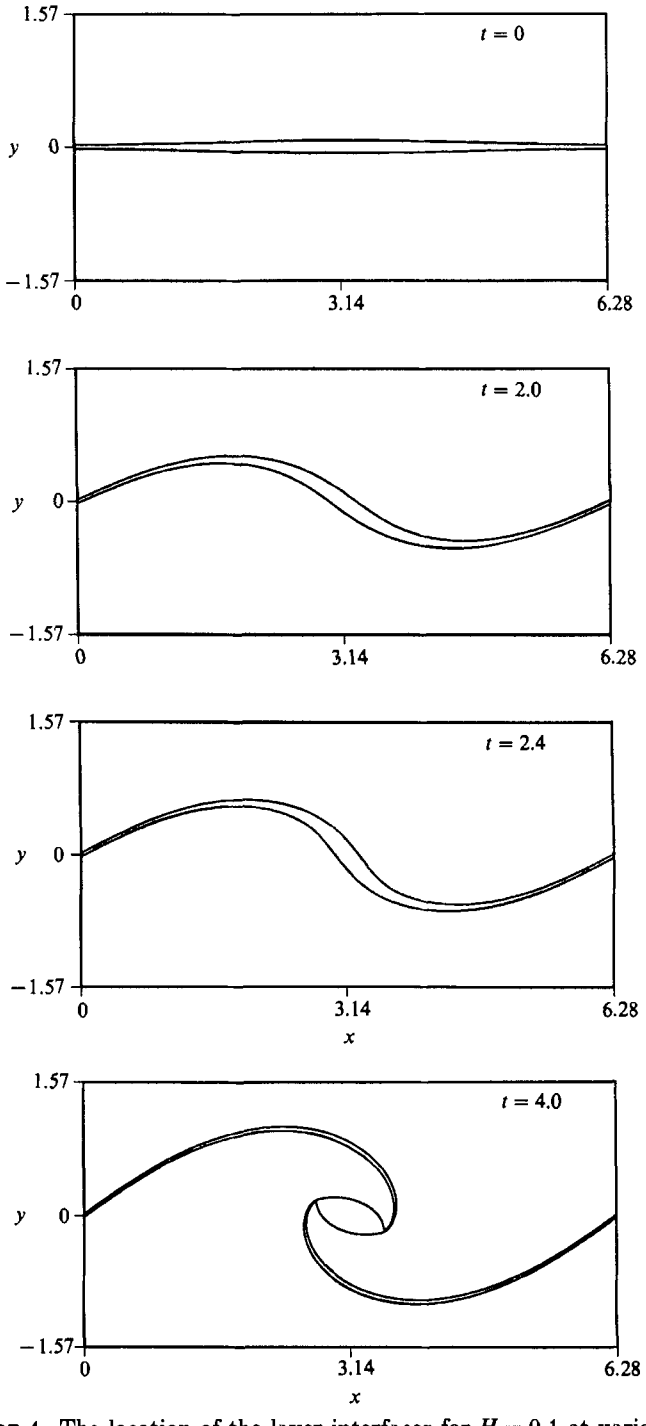

FIGURE 4. The location of the layer interfaces for $H = 0.1$ at various times.

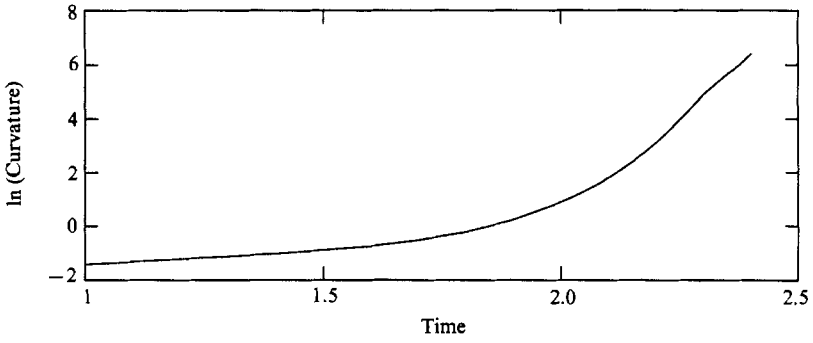

FIGURE 5. The evolution of the logarithm of the maximum curvature of the lower interface for $H = 0.025$.

more intense the vorticity, and the faster the vorticity advection and subsequent roll-up. Visually, the cores with their trailing arms are very similar to the structures observed by Zabusky *et al.* (1979) in their numerical simulation of the evolution of vortex patches. Our simulations also agree qualitatively with the vortex-layer simulations done by Pozrikidis & Higdon (1985), who used a different formulation and numerical method.

Owing to the nature of the vortex sheet singularity, the evolution of the interfacial curvature is of special interest. Using $H = 0.025$ as an example, it is apparent from figure 3 that the curvature grows rapidly in the region of the interface where the arms attach to the central core. Figure 5 displays the behaviour of the logarithm of the maximum curvature as a function of time. At first, the curvature grows only slowly, but then grows very rapidly as the core develops and the trailing arms begin to roll up. The logarithm of the maximum curvature shows only that the curvature is growing super-exponentially, but whether it becomes infinite in a finite time is unclear.

To gain more quantitative information concerning the regularity of the interfaces, we use the procedure employed by Sulem, Sulem & Frisch (1983). The decay of the computed spectra of the periodic function $Z(s,t) = z_1(s,t) - (2\pi/S)\,s$ is examined, where s is the arclength such that $s = 0$ at $p = 0$, and S is the arclength of a periodic segment of either interface. If $Z(s,t)$ is analytic in the strip, $\mathrm{Im}\, s \in (-\alpha, \bar{\alpha})$ in the complex s-plane, and has isolated branch-point singularities of order $\beta(t)-1, \bar{\beta}(t)-1$ on the lower, upper boundaries of the strip, then the asymptotic behaviour of the Fourier amplitudes, $A(k,t)$, is given by

$$|A(k,t)| \sim \begin{cases} \bar{C}(t)\,(-k)^{-\bar{\beta}(t)}\,\mathrm{e}^{\bar{\alpha}(t)\,k} & \text{as} \quad k \to -\infty \\ C(t)\,k^{-\beta(t)}\,\mathrm{e}^{-\alpha(t)\,k} & \text{as} \quad k \to +\infty. \end{cases} \tag{5.5}$$

This form for $A(k,t)$ is also suggested by the nature of the singularity for the vortex sheet. As long as α and $\bar{\alpha}$ are positive, the interfaces are analytic. If either α or $\bar{\alpha}$ vanish in finite time, then a branch-point singularity touches the real axis of the arclength and the layer interface has a singularity in its nth derivative, when n is the largest integer less than β or $\bar{\beta}$, respectively.

Values for α, $\bar{\alpha}$, β, $\bar{\beta}$, C, and $\bar{C}$ are obtained by a least-squares fit to the approximate spectra computed by the discrete Fourier transform. First, the interfaces are reparameterized in terms of the arclength. This is done by the procedure described in Appendix B. Enough points must be used in the arclength

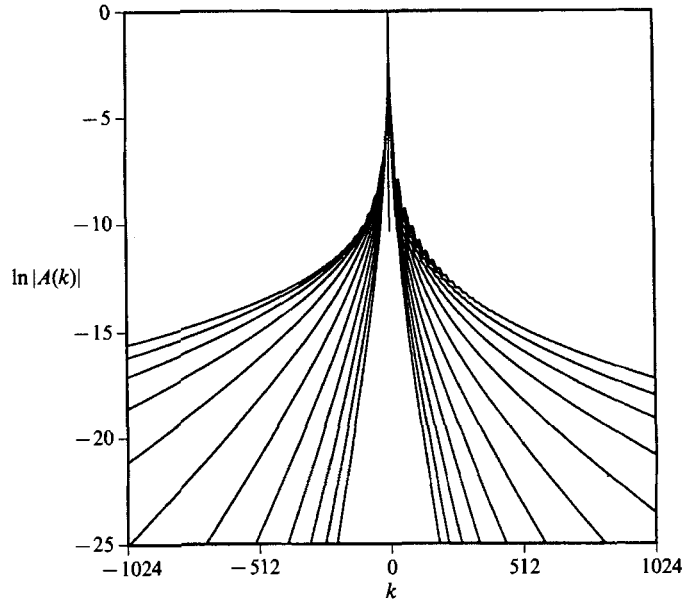

FIGURE 6. The Fourier spectra of the lower interface for $H = 0.025$, given at sequential times, starting at $t = 2.075$ in increments of 0.025 until $t = 2.375$.

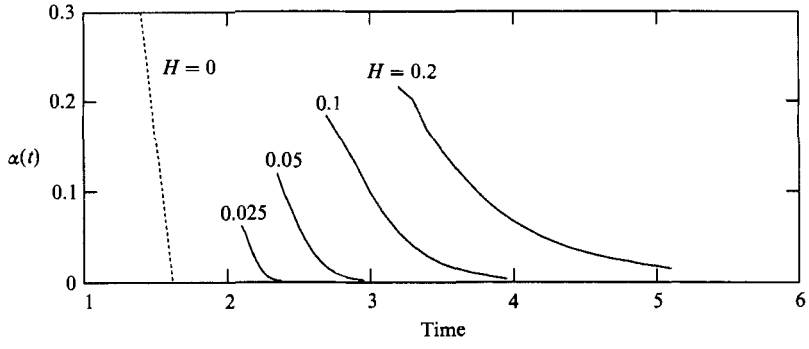

FIGURE 7. The evolution of α for various layer thicknesses. Also shown is the extrapolated behaviour of α for the vortex sheet (dashed curve).

representation to resolve the smallest scales that are present in the original parameterization. Figure 6 displays $\ln|A(k,t)|$ for the case $H = 0.025$. The profiles show a growth of the small scales in time.

The profiles in figure 6 are fitted to $\ln|A(k,t)|$, as given in (5.5), in the range $-18 < \ln|A(k,t)| < -15$, to determine α, $\bar{\alpha}$, β, $\bar{\beta}$, C, and $\bar{C}$. Using a nonlinear least-squares fit to $|A(k,t)|$ makes little difference to their values. As an indication of the accuracy of the fit, the average of the squared deviation for the least-squares fit to $\ln|A(k,t)|$ is less than 10^{-4}. In all cases, $\alpha = \bar{\alpha} > 0$ to within the accuracy of the fit. Figure 7 displays $\alpha(t)$ for several values of the mean thickness, $H = 0.025$, 0.05, 0.1, and 0.2. Although α becomes increasingly smaller, it does not seem to vanish in finite time. Also shown is the behaviour of α for the vortex sheet, obtained by extrapolation of numerical results for the evolution of the vortex sheet prescribed by (5.2). The curves for finite H have the appearance of nested hyperbolae with asymptotes, the time axis and the graph of $\alpha(t)$ for the vortex sheet. This behaviour signals again an

unusual limiting process. The results indicate that $\beta = 2.3 \pm 0.1$ and $\bar{\beta} = 1.7 \pm 0.1$ for large enough times, independently of the value for H. The value of β is close to that obtained in the case of the vortex sheet.

In conclusion, it appears that the interfaces remain analytic for all time during the evolution of vortex layers that start from initial conditions (5.1). Of course, several assumptions have been made. For example, we assume a certain form for the decay of the magnitude of the Fourier coefficients for the location of the interfaces. It is also assumed that there is no new, different behaviour in the motion of the layers at much later times. The issue here is that small scales, beyond the resolution of our calculations, may evolve into some structure with singularities. The results of Dritschel (1988) show that small protuberances on vortex patches may grow into long filaments. To the resolution of our calculations, no small protuberances formed on the layer boundaries. An examination of the surface rate of strain, defined by

$$St = \frac{x_p u_p + y_p v_p}{s_p^2}, \tag{5.6}$$

reveals that the interfaces stretch everywhere along the trailing arms, and compress only in a small region of the core adjacent to the point of high curvature where the trailing arms attach to the core. While surface stretching should act as a stabilizing agent (Moore & Griffith-Jones 1974), the trailing arms may not be stable until many more turns in the spiral are present (Moore 1976). The physical relevance of the presence of such instabilities will be discussed in §7.

6. The limit of vanishing thickness

In this section, the behaviour of the vortex layer is examined as its mean thickness is reduced, while its circulation around a periodic segment is held constant. For the initial conditions (5.1), the asymptotic analysis of §3 shows that the limiting behaviour is the vortex sheet considered by MBO, which acquires a singularity in finite time. The main objective in this study of the limiting behaviour of the vortex layer is the hope of elucidating the existence and nature of the vortex sheet beyond the singularity time.

From figures 3 and 4, it is clear that the central region of the layer has the most interesting behaviour. The trailing arms lie at a similar location for thinner layers, but the formation of the roughly elliptical cores, their size and orientation vary quite markedly. In figure 8, there are several sequences of layer profiles for various thicknesses, showing an enhanced view of the central region. Each column gives a sequence of layer positions at various times with H fixed, and goes as far as the computation is reliable, i.e. has at least 5 digits of accuracy in the perturbation kinetic energy. Each square is centred at $(\pi, 0)$ with sides of length $\frac{2}{3}\pi$. For a fixed time, beyond the critical time, the central region of the layers does not show a converging pattern, but at different times one can observe a similarity in the profiles. This non-uniform behaviour makes it very difficult to extrapolate the limiting behaviour from the profiles of the layer.

Instead, the limiting behaviour of certain curves internal to the layer are considered. The asymptotic analysis in §3 shows that both the material curve and the centre curve, defined by Moore (1978), will become the same vortex sheet as the layer in the limit. The first step then is to validate the asymptotic results by examining the limiting behaviour before the singularity time. Subsequently, the limit after the singularity time will be studied carefully.

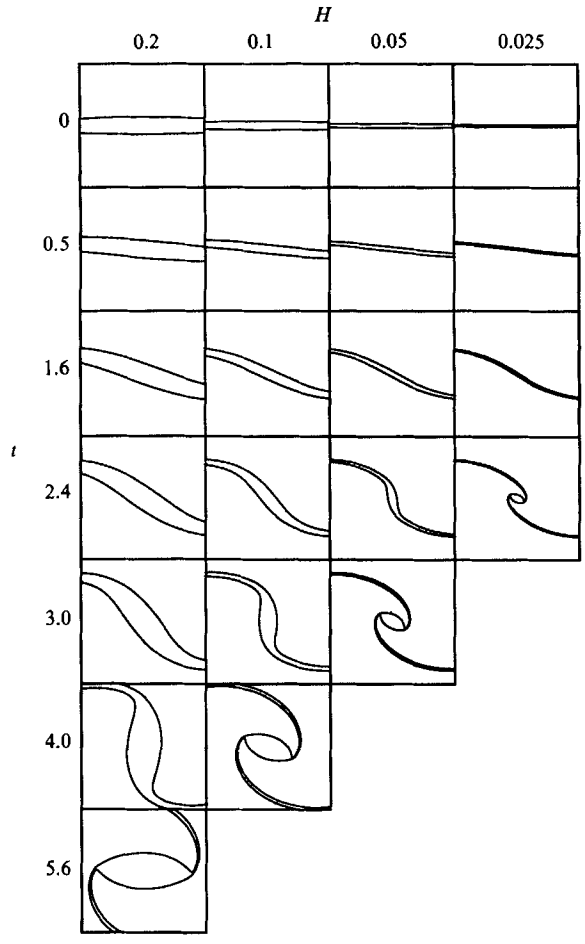

FIGURE 8. The core region of the layer interfaces for various times and thicknesses. Each box has dimensions, $\frac{2}{3}\pi$ by $\frac{2}{3}\pi$, and is centred at $(\pi, 0)$.

The location of the centre curve is determined at each time by the property that the two bounding interfaces lie an equal distance on either side of it along its normal. Specifically, given the layer interfaces z_1 and z_2, the quantities $\bar{z}_A(s), T_A(s)$, and $p_j(s)$ are found such that

$$z_j(p_j(s)) = \bar{z}_A(s) \mp \mathrm{i}\frac{T_A(s)}{2}\frac{\partial \bar{z}_A}{\partial s}(s) \quad \text{for} \quad j = 1, 2. \tag{6.1}$$

Here $\bar{z}_A(s)$ denotes the centre curve parametrized by its arclength s, $T_A(s)$ is the local thickness of the layer in the direction of the normal, $\mathrm{i}(\partial \bar{z}_A/\partial s)\,(s)$, and $p_j(s)$ relates the given parametrization of the bounding curves to the arclength of the centre curve. The upper, lower sign in (6.1) corresponds to $j = 1, 2$, respectively. Details of the construction of the centre curve are given in Appendix C. We define

$$\gamma_A(s) = T_A(s)\frac{2U}{H}. \tag{6.2}$$

Asymptotically, γ_A will approach the vortex sheet strength. Note that the position, $\bar{z}_A$, and γ_A are independent of H initially and are equal to the initial position and strength, respectively, of the vortex sheet prescribed in (5.2).

The other curve, $\bar{z}_B$, the material curve, moves with the fluid, and is found as the solution to the initial-value problem,

$$\frac{\partial \bar{z}_B}{\partial t}(p,t) = w(\bar{z}_B(p,t)), \quad \bar{z}_B(p,t=0) = p, \tag{6.3}$$

where the velocity, $w(\bar{z}_B(p,t))$, is given by (2.2). Some comments about the initial condition, (6.3), are in order. The asymptotic analysis does not indicate a preferred selection for the initial location of the material curve. Initial condition (6.3) is the obvious choice. Following the analysis in §3, we express the relationship between the material curve and the bounding curves as

$$z_j(p_j(p)) = \bar{z}_B(p) \mp \mathrm{i} H_j(p) \frac{\bar{z}_{Bp}(p)}{\bar{s}_{Bp}(p)}, \tag{6.4}$$

where H_j is the distance along the normal from the material curve to the jth bounding curve. The subscript p refers to differentiation. Given $z_j(p)$ and $\bar{z}_B$, the widths $H_j(p)$, and the mappings $p_j(p)$ are determined numerically using Newton's method. We define

$$\gamma_B(p) = T_B(p) \frac{2U}{H}, \tag{6.5}$$

where $T_B(p) = H_1(p) + H_2(p)$ is the local thickness. Asymptotically, γ_B approaches the vortex sheet strength. Note that γ_B is independent of H initially and equals the initial strength of the vortex sheet prescribed by (5.2). Since T_A and T_B are measured along the normals of different curves, γ_A and γ_B give different approximations to the vortex sheet strength.

As a verification of the asymptotic analysis in §3, the limiting behaviour of the two internal curves is considered at $t = 0.5$, which is well before the singularity time. In figure 9(*a*), the centre curve (solid) is shown for values of H that are successively halved. The convergence of the position of the centre curve to the position of the vortex sheet (dashed) is clearly linear in H as predicted by the asymptotic theory. Figure 9(*b*) shows the convergence of γ_A to the vortex sheet strength. Here the horizontal coordinate axis is given in the signed arclength from $p = \pi$ ($s = 0$). The position of the material curve and γ_B show the same behaviour. Again, the point-wise convergence to the vortex sheet is $O(H)$, consistent with the asymptotic theory.

Next, the limiting behaviour is considered at $t = 1.6$, which is just before the critical time of the vortex sheet. Figure 10 displays the same quantities as figure 9. The results for the material curve are again very similar to those for the centre curve. For both the centre and material curves, $\bar{z}$ and γ show an $O(H)$ convergence except near the vortex centre ($p = \pi$), which is the location of the vortex sheet singularity. Near the centre the convergence is not as apparent, but the difference between the results for successive halvings of the mean width is decreasing. We note also that the limiting behaviour of γ is consistent with the formation of a cusp in the vortex sheet strength at the centre (MBO; Moore 1979).

The more interesting questions involve the behaviour of the layer and the internal curves beyond the singularity time of the vortex sheet. As described in Appendix C, the set of nonlinear equations, (6.1), is solved to give the location of the centre curve. In figure 11, the centre curves are shown for the same vortex layers that are shown in figure 8. As H is reduced at a time beyond t_c, the behaviour of the centre curve becomes increasingly non-uniform, raising the question of whether a well-defined limit exists for the centre curve, and consequently for the layer.

We take particular note of the results at $t = 2.4$, the last time at which the

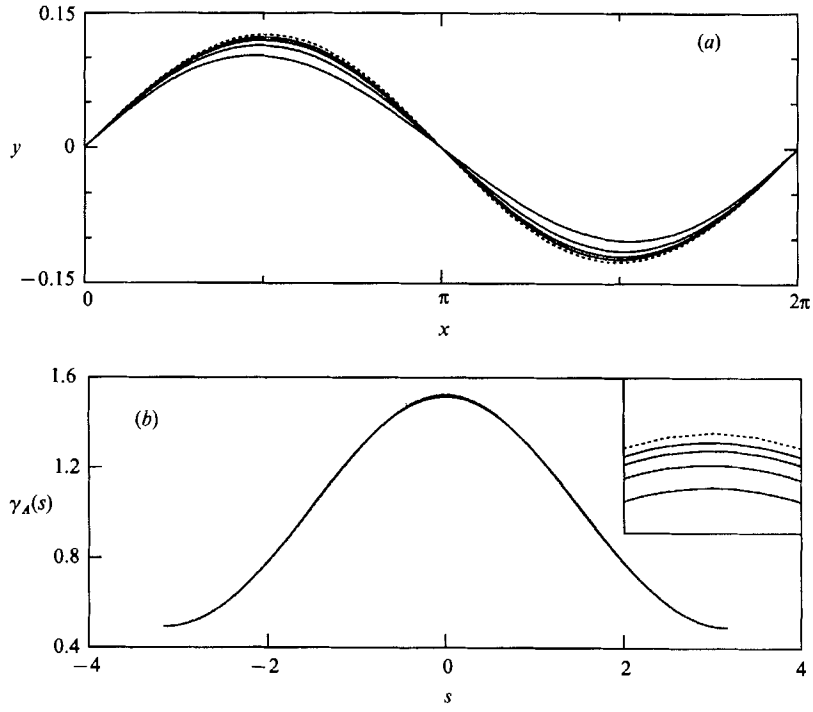

FIGURE 9. (*a*) The location of the centre curves (solid curves) at $t = 0.5$ for various thicknesses, $H = 0.2$, 0.1, 0.05, and 0.025. The sequence approaches the location of the vortex sheet (dashed curve). (*b*) The profiles of γ_A (solid curves) at $t = 0.5$ for various thicknesses, $H = 0.2$, 0.1, 0.05, and 0.025. The sequence approaches the profile of the vortex sheet strength (dashed curve). The inset gives an enlarged view with $-0.1 < s < 0.1$ and $1.505 < \gamma_A < 1.535$.

evolution of the layer is calculated reliably for all four values of H. In figure 12(*a*), the location of the centre curve is superimposed for the different values of H, showing clearly the convergence to a smooth curve away from the vortex core, but the profiles depend strongly on H near the core. In figure 12(*b*), γ_A is shown as a function of the signed arclength s at the same time, $t = 2.4$. While the non-uniform behaviour is again clearly apparent, more striking is the observation that γ_A is diverging at $s = 0$. For the thinnest layer, γ_A exhibits an interesting structure; from the high peak which occurs at the core centre, γ_A drops sharply to a local minimum where the trailing arms attach to the vortex core, and then climbs to another local maximum along the trailing arms. γ_A is converging on the trailing arms to a variation that has the same appearance as the strength of a vortex sheet that is developing a doubly branched spiral.

We consider now the behaviour of the material curve. In figure 13, the locations of the material curve are shown for the same vortex layers that are shown in figure 8, until $t = 2.4$. The behaviour of the material curve for $H = 0.025$ is generic and so we avoid the costly computation of its motion for the other layers at later times. The motion of the material curve emphasizes an important property of the motion of the layers. When the vortex core forms, it signals the transition from a flow that is mostly shearing to one that is mostly rotating in the core. Consequently, the material curve begins to wind up as a doubly branched spiral in the core on a timescale that is related to the vorticity in the core and which is much faster than the timescale for the trailing arms to roll up.

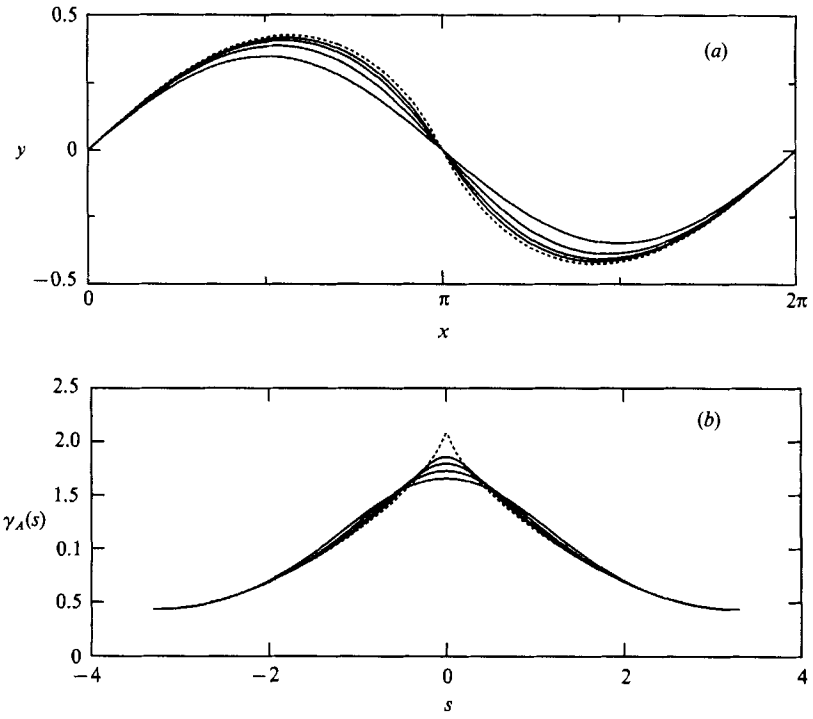

FIGURE 10. (*a*) The location of the centre curves at $t = 1.6$ for various thicknesses, $H = 0.2$, 0.1, 0.05, and 0.025. The sequence has increasing amplitude. (*b*) The profiles of γ_A at $t = 1.6$ for various thicknesses, $H = 0.2$, 0.1, 0.05, and 0.025. The sequence has increasing height.

Figure 14 displays the positions of the material curve at $t = 2.4$ for the different values of H. Like the centre curve, the locations of the material curve converge in regions away from $p = \pi$, but the convergence is increasingly non-uniform near the centre $p = \pi$ itself. The roll-up of the material curve invalidates the assumptions in the asymptotic analysis; the mappings $p_j(p)$ in (6.4) are no longer defined. In particular, for each value of H there is a critical time, t_B^c, at which the equations in (6.4) cease to have a solution at $p = \pi$, the location of the vortex sheet singularity. This time of failure, t_B^c, is shown in figure 15 for the different choices of H.

The breakdown in the assumptions of the asymptotic analysis for both internal curves is reflected in certain global properties of the layer. For example, the circulation around the core is proportional to the area of the core. The area of the core may be approximated by cutting off the trailing braids in the following manner. The points of maximum curvature on each bounding curve are joined by a straight line to the closest point on the opposite bounding curve. Once the vortex core forms, its area A, calculated in this fashion, stays constant in time to about three digits. The area is shown in figure 16 for the different values of H. Also shown is the curve $8.58H^{1.55}$, which is the best form fit with an algebraic power of H. The circulation, Γ, of the core is equal to $\omega A = 17UH^{0.55}$, which vanishes as $H \to 0$, pointing out that most of the vorticity is in the trailing arms.

The thickness of the core may be defined as double the least distance from the core centre to either of the bounding curves. The thickness is not steady, but appears to oscillate around a mean value. It is quite plausible that the cores are related to the family of rotating and oscillating ellipses in an external imposed strain, found by

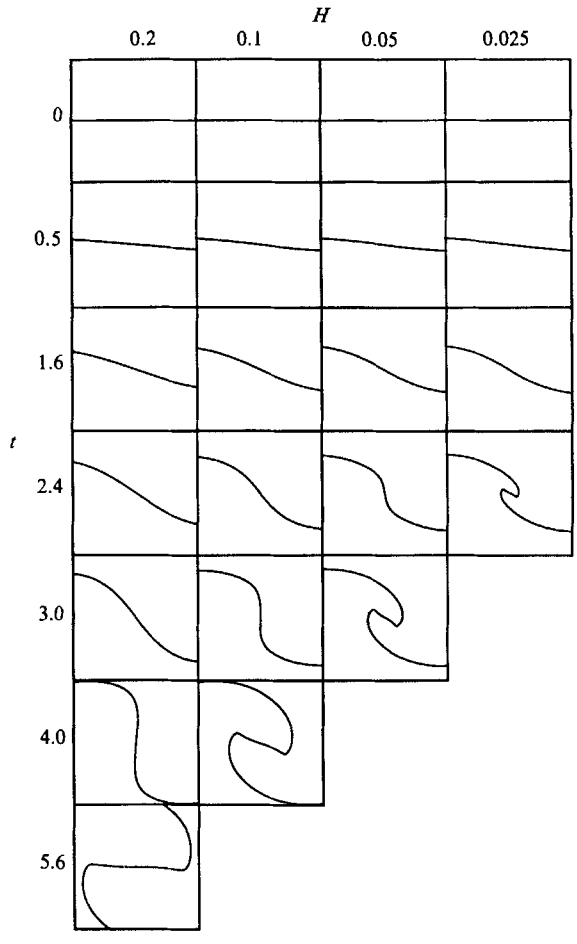

FIGURE 11. The core region of the centre curves for various times and thicknesses. The boxes are the same as those in figure 8.

Kida (1981). Here, the external imposed strain is induced in part by the rest of the layer.

The thickness of the core, T, is an important quantity since, on physical grounds, the thickness multiplied by the vorticity must give the vortex sheet strength at $p = \pi$ in the limit of vanishing thickness. In figure 17, we show $\gamma_T = 2UT/H$ as a function of time for the different values of H. Also, the critical time for the vortex sheet, as calculated by Shelley (1990), is drawn as a vertical, dashed line. Before the critical time, γ_T converges to the maximum vortex sheet strength, but after the critical time, it rises rapidly to a maximum and then begins, we believe, to oscillate. The maximum value of γ_T increases with a decrease in H, consistent with the behaviour of γ_A. An estimate for the thickness may be made based on the assumption that the cores are geometrically self-similar. Then, $T \approx A^{\frac{1}{2}} \approx H^{0.775}$, and so $\gamma_T \approx H^{-0.225}$.

7. Discussion and conclusions

We begin with the obvious: there is always some uncertainty about the validity of numerical results. We assume that the calculations capture all the important

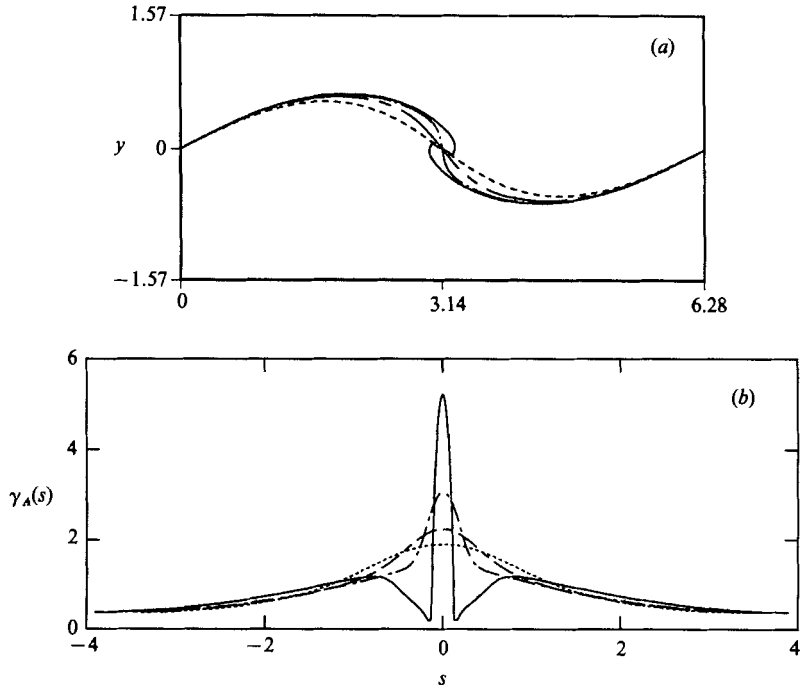

FIGURE 12. (*a*) The location of the centre curves at $t = 2.4$ for various thicknesses, $H = 0.2$ (dashed), 0.1 (chain-dashed), 0.05 (chain-dotted), and 0.025 (solid). (*b*) The profiles of γ_A at $t = 2.4$ for various thicknesses, $H = 0.2$ (dashed), 0.1 (chain-dashed), 0.05 (chain-dotted), and 0.025 (solid).

effects. Then the results indicate an important difference between vortex layers and vortex sheets. At the beginning, their evolutions are similar; a straining flow advects vorticity towards the central stagnation point. For the sheet, this results in the formation of a curvature singularity, while for the layer, vorticity accumulates into a new structure that changes the flow so that no new vorticity adds to the core subsequently. As the core rotates, the trailing arms are stretched and roll-up into a spiral.

For thinner layers, the core structure becomes a smaller fraction of the total layer. In fact, the core seems to collapse to a point with no circulation but infinite vortex sheet strength. If such a limit exists, it might be an example of a weak solution to the Euler equations described recently by Majda (1987). Presumably, this limit would not be a solution to the Birkhoff equation. Of course, the real question is the limiting behaviour of the solution to the Navier–Stokes equations at some fixed time after the singularity time, starting with the vortex sheet (5.2) as an initial condition. Our calculations show some agreement with the recent calculations by Bell, Colella & Glaz (1988) of the evolution of shear layers at high Reynolds number. Their calculations also show the formation of vortex cores, but this is not surprising since viscosity broadens the shear layers and strain flow will cause cores to form. Unfortunately, their results give no apparent limit as the Reynolds number is increased, but the calculations may be suffering from grid-induced modes that grow rapidly owing to the basic ill-posedness of the Kelvin–Helmholtz instability. We designed our numerical method to minimize the appearance of spurious small-scale modes due to truncation errors. If care is not taken, truncation errors will cause the mode with greatest growth rate to emerge rapidly in the calculations. The increasing

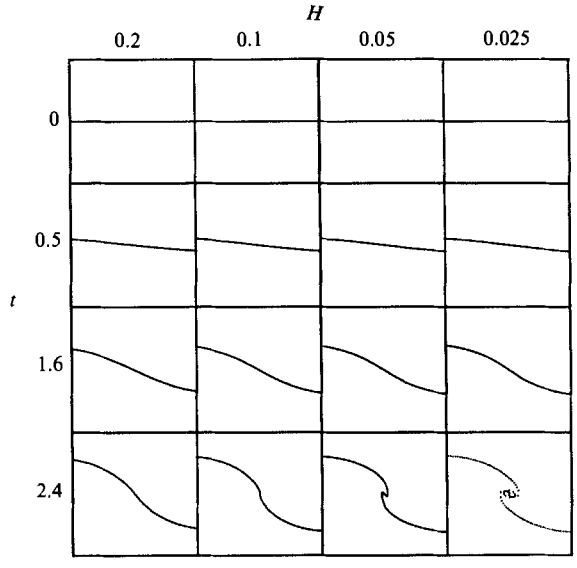

FIGURE 13. The core region of the material curves for various times and thicknesses. The boxes are the same as those in figure 8. Only the computational points are shown for the $t = 2.4$ and $H = 0.025$ case.

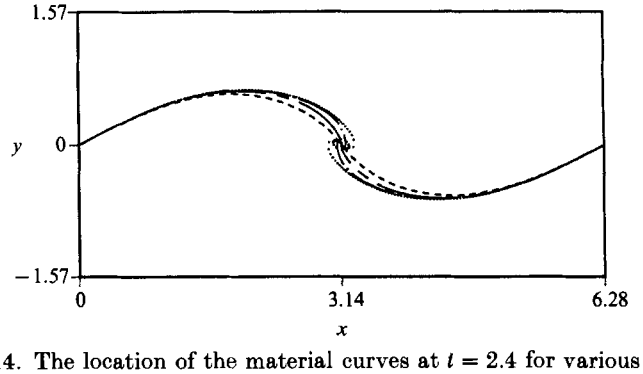

FIGURE 14. The location of the material curves at $t = 2.4$ for various thicknesses, $H = 0.2$ (dashed), 0.1 (chain-dashed), 0.05 (chain-dotted), and 0.025 (dotted).

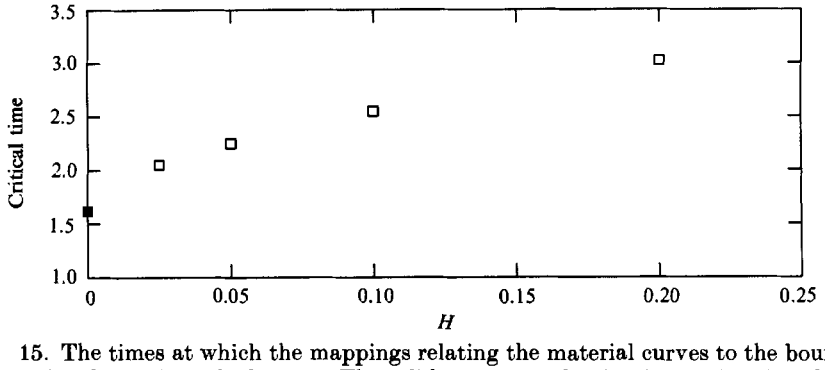

FIGURE 15. The times at which the mappings relating the material curves to the bounding curves cease to exist, for various thicknesses. The solid square marks the singularity time for the vortex sheet.

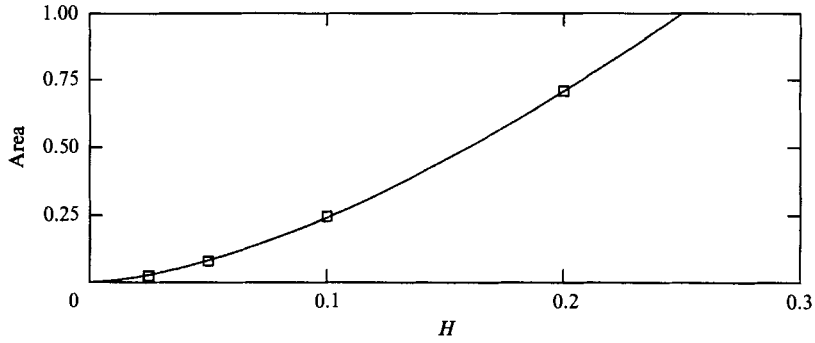

FIGURE 16. Core area for different thicknesses. The solid line is $8.58H^{1.55}$.

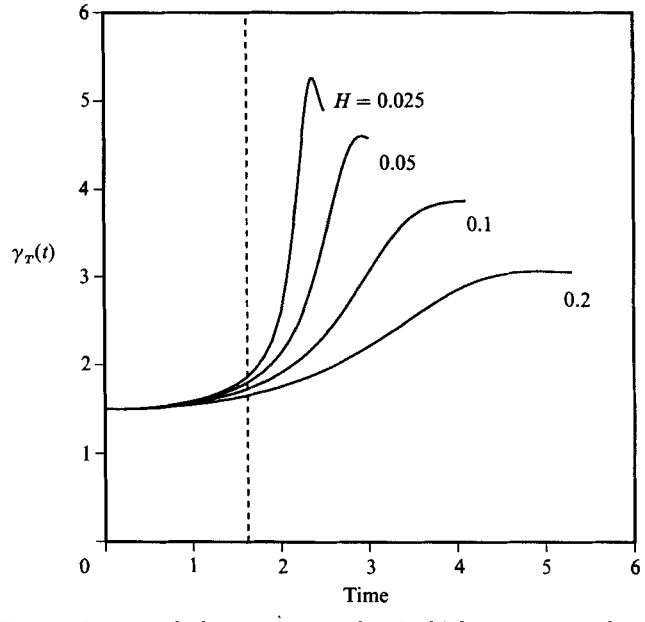

FIGURE 17. The evolution of the maximum local thickness times the absolute value of the vorticity, for various mean thicknesses. The dashed line marks the singularity time for the vortex sheet.

sensitivity of the motion of thinner layers to perturbations in their initial conditions indicates important dynamical behaviour of physical relevance.

If one accepts the crude analogy between our layer calculations and shear flow at high Reynolds number, then several important observations can be made. As already noted, viscosity will thicken the layer, and in the presence of a strain flow that compresses the layer tangentially, vortex cores will form owing to incompressibility. In general, the size of these cores will be related to the thickness of the viscous layer. Also, one may expect these cores to be at the centre of evolving, doubly branched spirals. Thus viscosity plays an early role in the rollup of vorticity, a possibility noted by Moore & Saffman (1973) in their work on the axial flow in laminar trailing vortices, although they sought a viscous solution at the centre of the spiral only after it had been formed. The strain flows that lead to the formation of vortex cores may arise from external conditions on the flow, such as the flow over wings, or they may arise locally from the development of unstable Kelvin–Helmholtz waves of small

wavelength. Once the cores have formed, they will interact with one another, merge in some cases and form larger structures.

Finally, we point out a similarity in our results with those of Krasny (1986*b*). One may interpret the smoothing parameter, δ, used in Krasny's work as a smearing of the vortex sheet; then the innermost turns of his spiral will lie effectively inside a vortex core, since the spacing between the turns is less than δ. In effect there are two regions in the spirals calculated by Krasny. The outer turns, which are independent of δ to a good approximation, agree with the limiting curve that we obtain for the centre curve or the material curve. The inner turns, which are dependent on δ, do not agree precisely with the material curve, but they do have some similarity with the spiral that the material curve forms inside the core. The behaviour of the material interface inside the core does bring up an important point with regard to the comparison with experiments. The motion of a material line, such as a dye streak, released initially within a thin vortex layer, may not indicate the true nature of the vorticity at later times when cores have formed.

This work has been partially supported by the National Science Foundation under Grants MCS-8302549 and DMS-8352067, and by the Office of Naval Research under Grants N00014-82-C-0451 and N00014-86-K-0759. Acknowledgement is made also to the National Center for Atmospheric Research, which is sponsored by the National Science Foundation, for some of the computing time used in this research.

Appendix A. The calculation of the perturbation kinetic energy

Pierrehumbert & Widnall (1981) show that the quantity

$$K = \omega \int_{R_2} \psi \, \mathrm{d}A \tag{A 1}$$

is a constant of the motion for vortex layers. K is the perturbation kinetic energy. The stream function ψ is continuous in the periodic strip and satisfies $\psi - U|y| \to 0$ as $|y| \to \infty$. Pierrehumbert & Widnall (1981) reduce the calculation of K to the evaluation of boundary integrals over Γ_1 and Γ_2, where the integrands have Cauchy and logarithmic singularities. Here, the evaluation of K will be recast so that only boundary integrals with Cauchy singularities need be evaluated, allowing use of the same adaptive quadrature methods as used in the calculation of the interfacial velocities, as discussed in §4.

First, by letting $f(y) = \frac{1}{2}y^2$ (so that $\Delta f = 1$), and then by using Green's second identity, the Divergence theorem, and the assumption of periodicity, (A 1) can be rewritten as

$$\begin{aligned}\frac{K}{\omega} &= -\omega \int_{R_2} f \, \mathrm{d}A + \int_{\Gamma_1+\Gamma_2} \left(\psi \frac{\partial f}{\partial n} - f \frac{\partial \psi}{\partial n}\right) \mathrm{d}s \\ &= -\omega \sum_{j=1}^{2} \int_0^{2\pi} [\pm \tfrac{1}{6} y_j^3(q)\, x_{jq}(q) \pm \psi_j(q)\, y_j(q)\, x_{jq}(q) - \tfrac{1}{2} y_j^2(q)\, (u_j(q)\, x_{jq}(q) + v_j(q)\, y_{jq}(q))] \, \mathrm{d}q.\end{aligned} \tag{A 2}$$

The upper and lower signs are taken with $j = 1$ and 2 respectively. Since the integrands are periodic and given at uniformly spaced values of q, the integrals in (A 2) can be calculated with spectral accuracy by the trapezoidal rule. The interfacial velocities, $u_j(q)$ and $v_j(q)$, are calculated from the interfacial positions, $x_j(q)$ and $y_j(q)$,

by (2.4) with adaptive quadrature methods. The stream function ψ_j along Γ_j may be calculated from

$$\psi_j(q) = \psi_j(0) + \int_0^q u_j(p)\, y_{jp}(p) - v_j(p)\, x_{jp}(p))\, \mathrm{d}p.$$

The indefinite integral is evaluated with spectral accuracy, at evenly spaced values of q, using the discrete Fourier transform. Thus, to complete the calculation of K, $\psi_j(0)$ must be found.

$\psi_j(0)$ is calculated by means of a distribution of dipoles along each interface. Namely,

$$\psi(x, y) = \bar{\psi}(y) + \mathrm{Re}\{\Psi(x + \mathrm{i}y)\}, \tag{A 3}$$

where

$$\bar{\psi} = \begin{cases} -Uy & \text{in } R_1 \\ \dfrac{U}{H} y^2 + \dfrac{UH}{4} & \text{in } R_2 \\ Uy & \text{in } R_3 \end{cases} \tag{A 4}$$

(see figure 1 for definitions of R_j) and

$$\Psi(\eta = x + \mathrm{i}y) = \sum_{j=1}^{2} \int_0^{2\pi} (\mu_j(q) + \mathrm{i}\nu_j(q))\, \mathrm{P}(\eta, z_j(q))\, z_{jq}(q)\, \mathrm{d}q. \tag{A 5}$$

The complex dipole strength is given by $\mu_j(q) + \mathrm{i}\nu_j(q)$. Note that once μ_j and ν_j are determined, $\Psi(z_j(0))$ may be calculated using the same quadrature methods as used in calculating the velocity. The requirement of continuity of ψ at the interfaces Γ_1 and Γ_2 determines μ_j as

$$\mu_j(q) = U\left(y_j(q) \pm \frac{1}{H} y_j^2(q) \pm \frac{H}{4}\right),$$

while the requirement of continuity of tangential velocity yields

$$\nu_{jq}(q) = -U\left(1 \pm \frac{2}{H} y_j(q))\, x_{jq}(q)\right).$$

The integration of ν_{jq} is done numerically, with spectral accuracy, by use of the discrete Fourier transform. Fortunately, the constant of integration is unimportant since, for all η,

$$\mathrm{Im}\left\{\int_0^{2\pi} \mathrm{P}(\eta, z_j(q))\, z_{jq}(q)\, \mathrm{d}q\right\} = 0.$$

Finally, we note that $\bar{\psi}$ satisfies the far-field boundary conditions on ψ, so $\mathrm{Re}\{\Psi\}$ must vanish as $|y| \to \infty$. This is true if the y-moment of the vorticity in a periodic strip (which is constant of the motion) is zero. The set of initial conditions considered here satisfies this constraint.

Appendix B. The method of grid redistribution

The method of equidistributing meshes is adapted to parametrized curves in R^2. For discussion and examples of equidistributing meshes for functions of a single variable, see Hyman & Naughton (1984).

To be specific, let $\Gamma(p) = (x(p), y(p))$ be a curve that is closed, or periodic in the x-direction, with $0 \leqslant p \leqslant 2\pi$. Γ can also be parametrized as $\Gamma(s(p))$ where $s(p)$ is the arclength measured from $p = 0$. Let $F(s)$ be a strictly positive, periodic function that in some sense measures where Γ needs to be resolved by a mesh. In particular, large

or small values of Fs_p indicate the sections of Γ where more or less collocation points are required. When Γ is not well-resolved in this sense, we seek a new parametrization, $\Gamma(s(p'))$, with the old and new parametrizations related by

$$p' = f(p) \quad \text{with} \quad f(0) = 0, \tag{B 1}$$

such that

$$F(s(p'))\, s_{p'} = \langle F \rangle, \tag{B 2}$$

where

$$\langle F \rangle = \frac{1}{2\pi} \int_0^{2\pi} F(s(p))\, s_p \, dp. \tag{B 3}$$

Thus, a new parametrization is sought such that Fs_p is everywhere equal to its mean $\langle F \rangle$, which is independent of parametrization. This is the method of equidistributing meshes.

Using the relation, $s_{p'}\, df/dp = s_p$, (B 2) becomes

$$\frac{df}{dp}(p) = \frac{F(s(p))\, s_p(p)}{\langle F \rangle} \tag{B 4}$$

or, upon integration,

$$f(p) = \frac{1}{\langle F \rangle} \int_0^p F(s(q))\, s_q(q)\, dq. \tag{B 5}$$

Thus, the mapping from p to p' is completely specified. If the current parametrization is non-singular, i.e. $s_p > 0$, then since $F(s(p)) > 0$ by assumption, f is a strictly monotonic function of p, with $f(0) = 0$ and $f(2\pi) = 2\pi$. Thus, f maps $[0, 2\pi]$ onto itself, and is one-to-one.

Let N be the number of points being used in the calculation, with $h = 2\pi/N$. We seek the values of p at which the new parameter p' is evenly spaced. That is, find the sequence $\{p_k\}_{k=0}^N$ with $p_0 = 0$ such that

$$kh = f(p_k) = \frac{1}{\langle F \rangle} \int_0^{p_k} F(s(q))\, s_q(q)\, dq. \tag{B 6}$$

This equation is solved by Newton's method for successive values of p_k. In order to use Newton's method, the indefinite integral must be evaluated at points other than the collocation points. At the collocation points, the indefinite integral is evaluated easily by the discrete Fourier transform of the integrand. We use the Hermite interpolation method, based on iterated, quintic splines described in Shelley & Baker (1988), to evaluate the integral at other points. Once the sequence $\{p_k\}$ is determined, $\Gamma(p_k)$ is found by Hermite interpolation.

We use the following F:

$$F(s) = \frac{1}{\langle 1 \rangle} + w \frac{(\kappa^2(s) + \epsilon^2)^{\frac{1}{2}}}{\langle (\kappa^2 + \epsilon^2)^{\frac{1}{2}} \rangle}, \tag{B 7}$$

where $\kappa(s)$ is the curvature. Note that if (i) $\kappa = 0$ (Γ is a flat surface), (ii) κ is a constant (Γ is a circle), or (iii) $w = 0$, then $F(s)$ is a constant, and the new parametrization will be equally spaced in arclength. Case (iii) is used for parametrizing the layer interfaces in the arclength coordinate for the spectral analysis in §5. When $\kappa \neq 0$ and $w \neq 0$, then a weighting is given to curvature, and the redistribution method tries to resolve regions of high curvature. For our work, we use $\epsilon = 0.001$ and $w = 1$. These values are found by experimentation to work well.

For time-dependent problems, it is important that the new parametrization remains accurate for at least a short while. For this, it is necessary to smooth F so

that its influence extends to a small neighbourhood in case the motion shifts F. We choose to smooth F by convolution with a narrowly peaked, periodic function,

$$(\sin\tfrac{1}{2}(p-\alpha\sin p))^{(2k)}, \tag{B 8}$$

with $k = 6$ and $\alpha = 0.95$.

Appendix C. The determination of the centre curve

In this Appendix, we describe the construction of centre curves for vortex layers. Given two non-intersecting, bounding curves (the layer interfaces), the centre curve is determined by the property that the two bounding curves lie an equal distance on either side of it along its normal; hence (6.1). We recast (6.1) into a pair of coupled ordinary differential equations for the mappings, $p_j(s)$, $j = 1, 2$, which relate the arclength parametrization of the centre curve $(\bar{x}(s), \bar{y}(s))$ to the given parametrizations of the bounding curves $(x_j(p_j), y_j(p_j))$, $j = 1, 2$, so that $(x_j(p_j(s)), y_j(p_j(s)))$ lies on the normal from the centre curve at $(\bar{x}(s), \bar{y}(s))$. First, by adding the equations in (6.1), we obtain

$$x_1(p_1(s))+x_2(p_2(s))-2\bar{x}(s) = 0, \quad y_1(p_1(s))+y_2(p_2(s))-2\bar{y}(s) = 0. \tag{C 1a, b}$$

Then, by subtracting the equations, we obtain

$$\frac{\mathrm{d}\bar{x}}{\mathrm{d}s}(s) = -\frac{\Delta y}{T_A}, \quad \frac{\mathrm{d}\bar{y}}{\mathrm{d}s}(s) = \frac{\Delta x}{T_A}, \tag{C 1c, d}$$

where $\Delta x = x_1(p_1(s))-x_2(p_2(s))$, $\Delta y = y_1(p_1(s))-y_2(p_2(s))$, and $T_A = (\Delta x^2+\Delta y^2)^{\frac{1}{2}}$. In principle, the centre curve could be solved from (C 1) as a nonlinear boundary-value problem, given boundary conditions that imply periodicity of the centre curve. However, we find it simpler to convert (C 1) into a set of ordinary differential equations and solve for the centre curve by a parallel shooting method.

For the sake of brevity, dependence on $p_j(s)$ will no longer be shown explicitly. Differentiation of (C 1a) and (C 1b) with respect to s, and use of (C 1c) and (C 1d) leads to the following system of linear equations for $(\mathrm{d}p_1/\mathrm{d}s)(s)$ and $(\mathrm{d}p_2/\mathrm{d}s)(s)$:

$$\frac{\mathrm{d}x_1}{\mathrm{d}p_1}\frac{\mathrm{d}p_1}{\mathrm{d}s}+\frac{\mathrm{d}x_2}{\mathrm{d}p_2}\frac{\mathrm{d}p_2}{\mathrm{d}s} = -\frac{2\Delta y}{T_A}, \quad \frac{\mathrm{d}y_1}{\mathrm{d}p_1}\frac{\mathrm{d}p_1}{\mathrm{d}s}+\frac{\mathrm{d}y_2}{\mathrm{d}p_2}\frac{\mathrm{d}p_2}{\mathrm{d}s} = \frac{2\Delta x}{T_A}. \tag{C 2a, b}$$

If the determinant of this system, $D = (\mathrm{d}x_1/\mathrm{d}p_1)(\mathrm{d}y_2/\mathrm{d}p_2)-(\mathrm{d}x_2/\mathrm{d}p_2)(\mathrm{d}y_1/\mathrm{d}p_1)$, is non-zero, (C 2) can be inverted for $\mathrm{d}p_1/\mathrm{d}s$ and $\mathrm{d}p_2/\mathrm{d}s$ as

$$\frac{\mathrm{d}p_1}{\mathrm{d}s} = -\frac{2}{T_A}\frac{\dfrac{\mathrm{d}x_2}{\mathrm{d}p_2}\Delta x+\dfrac{\mathrm{d}y_2}{\mathrm{d}p_2}\Delta y}{D}, \quad \frac{\mathrm{d}p_2}{\mathrm{d}s} = \frac{2}{T_A}\frac{\dfrac{\mathrm{d}x_1}{\mathrm{d}p_1}\Delta x+\dfrac{\mathrm{d}y_1}{\mathrm{d}p_1}\Delta y}{D}. \tag{C 3a, b}$$

We seek a solution to this system that will yield a periodic centre curve. Unfortunately, it is not clear that such a solution exists or is unique. The major difficulty is that D may vanish. There are points of symmetry for the centre curve, namely at the centre of the core ($x = \pi$) and the midpoint along the trailing arm connecting two cores ($x = 0$ or 2π), at which points D vanishes, and, if the centre curve exists, there must be a compensating zero in the numerators of (C 3). These conditions determine p_1 and p_2. We call the points where D and the numerators vanish indeterminate points. Note that these particular indeterminate points occur where the minimum distance between the bounding curves has local extrema.

Furthermore, assuming that the zeros in D and the numerators are simple in s, say at $s = 0$ for convenience, we expand the right-hand side of (C 3) around $s = 0$, and examine the limiting expression as s is taken to zero. This yields two coupled equations for $\mathrm{d}p_1/\mathrm{d}s$ and $\mathrm{d}p_2/\mathrm{d}s$ at $s = 0$, which can be solved explicitly as

$$\frac{\mathrm{d}p_1}{\mathrm{d}s} = K\frac{2}{R}\frac{aK-b}{cK+d}, \quad \frac{\mathrm{d}p_2}{\mathrm{d}s} = \frac{2}{R}\frac{aK-b}{cK+d}, \tag{C 4a, b}$$

where

$$a = \frac{\mathrm{d}x_1}{\mathrm{d}p_1}\frac{\mathrm{d}x_1}{\mathrm{d}p_1} + \frac{\mathrm{d}y_1}{\mathrm{d}p_1}\frac{\mathrm{d}y_1}{\mathrm{d}p_1} + \frac{\mathrm{d}^2x_1}{\mathrm{d}p_1^2}\Delta x + \frac{\mathrm{d}^2y_1}{\mathrm{d}p_1^2}\Delta y,$$

$$b = \frac{\mathrm{d}x_1}{\mathrm{d}p_1}\frac{\mathrm{d}x_2}{\mathrm{d}p_2} + \frac{\mathrm{d}y_1}{\mathrm{d}p_1}\frac{\mathrm{d}y_2}{\mathrm{d}p_2}, \quad c = \frac{\mathrm{d}^2x_1}{\mathrm{d}p_1^2}\frac{\mathrm{d}y_2}{\mathrm{d}p_2} - \frac{\mathrm{d}^2y_1}{\mathrm{d}p_1^2}\frac{\mathrm{d}x_2}{\mathrm{d}p_2}, \quad d = \frac{\mathrm{d}x_1}{\mathrm{d}p_1}\frac{\mathrm{d}^2y_2}{\mathrm{d}p_2^2} - \frac{\mathrm{d}y_1}{\mathrm{d}p_1}\frac{\mathrm{d}^2x_2}{\mathrm{d}p_2^2},$$

$$e = \frac{\mathrm{d}x_2}{\mathrm{d}p_2}\frac{\mathrm{d}x_2}{\mathrm{d}p_2} + \frac{\mathrm{d}y_2}{\mathrm{d}p_2}\frac{\mathrm{d}y_2}{\mathrm{d}p_2} - \frac{\mathrm{d}^2x_2}{\mathrm{d}p_2^2}\Delta x - \frac{\mathrm{d}^2y_2}{\mathrm{d}p_2^2}\Delta y,$$

and

$$K = (e/b)^{\frac{1}{2}}.$$

Before the establishment of the cores, we use the indeterminate points at $x = 0$ and $x = 2\pi$ as initial points and integrate (C 3) numerically towards the centre. We find, by experimentation and the consideration of a model problem involving two parabolae for the bounding curves, that the integration is stable numerically only when (C 3) is solved in the direction for which the bounding curves are separating. The two curves match at the indeterminate point at the centre. When the cores have developed, four new indeterminate points arise, located at local extrema in the minimum distance between the bounding curves. Two of them, located near the attachment of the trailing arms to the core, are points from which the centre curve can be integrated stably. The curves constructed by integration from the points at $x = 0$, $x = 2\pi$, and the points near the attachment of the trailing arms to the core match at the core centre and at the remaining indeterminate points along the trailing arms.

For the results reported in §6, the numerical integration is based on the fourth-order, Adams–Moulton predictor-corrector with a step-size of 10^{-6} in the arclength. The initial points are located a short distance from the indeterminate points. More details and a deeper discussion of the nature of the centre curve will be given elsewhere.

REFERENCES

Baker, G. R. & Shelley, M. J. 1986 Boundary integral techniques for multi-connected domains. *J. Comput. Phys.* **64**, 112.

Bell, J. B., Colella, P. & Glaz, H. M. 1988 A second-order projection method for the incompressible Navier–Stokes equations. *Lawrence Livermore National Laboratory Preprint* UCRL-98225.

Broadbent, E. G. & Moore, D. W. 1985 Waves of extreme form on a layer of uniform vorticity. *Phys. Fluids* **28**, 1561.

Caflisch, R. & Orellana, O. 1986*a* Long time existence for a slightly perturbed vortex sheet. *Commun. Pure Appl. Maths* **39**, 807.

Caflisch, R. & Orellana, O. 1989 Singularity formation and ill-posedness for vortex sheets. *SIAM J. Math. Anal.* **20**, 293.

Diperna, R. & Majda, A. 1987 Concentrations in regularizations for 2-d incompressible flow. *Commun. Pure Appl. Maths* **40**, 301.

DRITSCHEL, D. G. 1988 The repeated filamentation of two-dimensional vorticity interfaces. *J. Fluid Mech.* **194**, 511.

DRITSCHEL, D. G. 1990 The stability of elliptical vortices in an external straining flow. *J. Fluid Mech.* **210**, 223.

DUCHON, R. & ROBERT, R. 1989 Global vortex sheet solutions to Euler equations in the plane. *Commun. Partial Diff. Equn* (to appear).

HIGDON, J. J. L. & POZRIKIDIS, C. 1985 The self-induced motion of vortex sheets. *J. Fluid Mech.* **150**, 203.

HYMAN, J. M. & NAUGHTON, M. J. 1984 Static rezone methods for tensor-product grids. In *Proc. SIAM–AMS Conf. on Large Scale Computation in Fluid Mechanics*. Philadelphia: SIAM.

KIDA, S. 1981 Motion of an elliptic vortex in a uniform shear flow. *J. Phys. Soc. Japan* **50**, 3517.

KRASNY, R. 1986*a* A study of singularity formation in a vortex sheet by the point-vortex approximation. *J. Fluid Mech.* **167**, 65.

KRASNY, R. 1986*b* Desingularization of periodic vortex sheet roll-up. *J. Comput. Phys.* **65**, 292.

LOVE, A. E. H. 1883 On the stability of certain vortex motions. *Proc. R. Soc. Lond.* A **25**, 18.

MAJDA, A. 1987 Vortex dynamics: Numerical analysis, scientific computing, and mathematical theory. In *Proc. First Intl Conf. on Industrial and Applied Maths, Paris.*

MCGRATH, F. J. 1967 Nonstationary plane flow of viscous and ideal fluids. *Arch. Rat. Mech. Anal.* **27**, 329.

MEIRON, D. I, BAKER, G. R. & ORSZAG, S. A. 1982 Analytic structure of vortex sheet dynamics. Part 1. Kelvin–Helmholtz instability. *J. Fluid Mech.* **114**, 283 (referred to as MBO).

MOORE, D. W. 1976 The stability of an evolving vortex sheet. *Mathematika* **23**, 35.

MOORE, D. W. 1978 The equation of motion of a vortex layer of small thickness. *Stud. Appl. Maths* **58**, 119.

MOORE, D. W. 1979 The spontaneous appearance of a singularity in the shape of an evolving vortex sheet. *Proc. R. Soc. Lond.* A **365**, 105.

MOORE, D. W. 1985 Numerical and analytical aspects of Helmholtz instability. In *Theoretical and Applied Mechanics, Proc.* XVI IUTAM (ed. Niodson & Olhoff), p. 263. North-Holland.

MOORE, D. W. & GRIFFITH-JONES, R. 1974 The stability of an expanding circular vortex sheet. *Mathematika* **21**, 128.

MOORE, D. W. & SAFFMAN, P. G. 1973 Axial flow in laminar trailing vortices. *Proc. R. Soc. Lond.* A **346**, 491.

PIERREHUMBERT, R. T. & WIDNALL, S. E. 1981 The structure of organized vortices in a free shear layer. *J. Fluid Mech.* **102**, 301.

POZRIKIDIS, C. & HIGDON, J. J. L. 1985 Nonlinear Kelvin–Helmholtz instability of a finite vortex layer. *J. Fluid Mech.* **157**, 225.

PULLIN, D. I. 1981 The nonlinear behaviour of a constant vorticity layer at a wall. *J. Fluid Mech.* **108**, 401.

PULLIN, D. I. & JACOBS, P. A. 1986 Inviscid evolution of stretched vortex arrays. *J. Fluid Mech.* **171**, 377.

PULLIN, D. I. & PHILLIPS, W. R. C. 1981 On a generalization of Kaden's problem. *J. Fluid Mech.* **104**, 45.

RAYLEIGH, LORD 1880 On the stability or instability of certain fluid motions. *Proc. Lond. Math. Soc.* **11**, 57.

SAFFMAN, P. G. & BAKER, G. R. 1979 Vortex interactions. *Ann. Rev. Fluid Mech.* **11**, 95.

SHELLEY, M. J. 1990 A study of singularity formation in vortex sheet motion by a spectrally accurate vortex method. *J. Fluid Mech.* (submitted).

SHELLEY, M. J. & BAKER, G. R. 1988 Order conserving approximations to derivatives of periodic functions using iterated splines. *SIAM J. Num. Anal.* **25**, 1442.

SMITH, J. H. B. 1986 Vortex flows in aerodynamics. *Ann. Rev. Fluid Mech.* **18**, 221.

SULEM, C., SULEM, P. L., BARDOS, C. & FRISCH, U. 1981 Finite time analyticity for the two and three dimensional Kelvin–Helmholtz instability. *Commun. Math. Phys.* **80**, 485.

SULEM, C., SULEM, P. L. & FRISCH, H. 1983 Tracing complex singularities with spectral methods. *J. Comput. Phys.* **50**, 138.

VAN DYKE, M. 1975 *Perturbation Methods in Fluid Mechanics.* Parabolic.

YUDOVICH, V. I. 1963 Non-stationary flow of an ideal incompressible liquid. *Zh. Vych. Mat.* **3**, 1032.

ZABUSKY, N. J., HUGHES, M. H. & ROBERTS, K. V. 1979 Contour dynamics for the Euler equations in two dimensions. *J. Comput. Phys.* **30**, 96.